

HEAT TRANSFER MODELING AND USE OF DISTRIBUTED
TEMPERATURE MEASUREMENTS TO PREDICT RATE

A Thesis

by

GIBRAN MUSHTAQ HASHMI

Submitted to the Office of Graduate and Professional Studies of
Texas A&M University
in partial fulfillment of the requirements for the degree of

MASTER OF SCIENCE

Chair of Committee,	Abu Rashid Hasan
Committee Members,	Hadi Nasrabadi
	Nazmul Karim
Head of Department,	A. D. Hill

August 2014

Major Subject: Petroleum Engineering

Copyright 2014 Gibran Mushtaq Hashmi

ABSTRACT

Heat transfer modeling is important in many fields of engineering. In petroleum engineering, heat transfer modeling has many applications. One such application that this study focused on is flow rate estimation. In this work, two different models for estimating wellbore fluid temperature are highlighted with emphasis on using those models along with distributed temperature measurements to estimate rate of flow.

Both models employ mass, momentum and energy balance and are well established in the literature. The *steady-state model* is used where the fluid flow is essentially steady and any change in rate is followed by a sufficiently long steady schedule. The *transient model* is used where the well is still flowing in the initial stages or fluctuations in rate cause time of flow to be an important consideration. Flow rate estimation is predicated on the match between the measured and the estimated fluid temperatures.

Superposition of heat flow is developed in this work with regards to both steady-state and transient wellbore fluid temperature models. The superposition principle accounts for the changing heat transfer rate between wellbore fluid and formation which all flowing fluid temperature models in literature neglect.

Three case studies are presented to demonstrate the application of the methodology of rate estimation proposed. Fluid flow rates for steady and transient cases were

successfully estimated within engineering accuracy for all three cases. In all three cases, in addition to the traditional downhole-pressure and surface-rate measurements, temperatures were recorded at various depths providing the data that allowed for testing of the models. The computational accuracy of flow rates increased at shallower depths owing to the increased heat transfer that was conducive to larger temperature differences, enhancing the fidelity of measurements.

The analysis also provides an opportunity to consider its use in other applications such as pre-cleanup transient testing. Computed rates from the proposed methodology can be used to perform transient analysis for the cleanup period. While the field examples strengthened the new rate-computation methods introduced here, simulated example shown at the end of the study probed the possibility of extracting meaningful information from the cleanup data.

DEDICATION

To my parents, fiancée and siblings.

ACKNOWLEDGEMENTS

My special thanks go to my advisor, Dr. A. R. Hasan, who not only financially supported but also encouraged and helped me throughout this project. His insightful implementations of the ideas often led to important improvements. Without his guidance and patience, this work would never be fulfilled. He was a constant support in times of stress, not only in the matters of academics but also provided healthy advice in financial matters.

I also wish to thank the Department of Petroleum Engineering at Texas A&M University for the role they played in the financial support given to me and all my teachers whose valuable lessons led me to attain better understanding of the petroleum engineering concepts in order to successfully complete this task.

Well-deserved thanks extend to Mr. Shah Kabir of Hess Corporation who provided us with excellent technical assistance and field data that enabled us to test our models. His constant encouragement and comments help improve this work considerably.

I especially wish to thank Dr. Hadi Nasrabadi and Dr. Nazmul Karim for agreeing to serve on my committee.

I also want to thank my research group members and friends for their support and suggestions. They were often the people to provide initial feedback or suggest improvements whenever I got stuck.

Finally I wish to express my gratitude to my parents who encouraged me at each step and helped me throughout my entire course of study. Their emotional support meant the world at times. My siblings also provided deep moral support and encouragement. I also wish to thank my fiancée for her support and patience.

NOMENCLATURE

a	Lumped parameter defined by Eq. 32, hr^{-1}
B	Lumped parameter defined by Eq. 21, $\text{Btu/hr.ft.}^\circ\text{F}$
C_J	Joule-Thomson coefficient, $^\circ\text{F}/(\text{lb}_f/\text{ft}^2)$
c_p	Tubing fluid heat capacity, $\text{Btu/lbm } ^\circ\text{F}$
C_T	Thermal storage parameter, dimensionless
dp/dz	Tubing pressure gradient, psi/ft
g	Gravitational acceleration, ft/sec^2
g_c	Conversion factor, $32.17 (\text{lbm-ft})/\text{lbf/sec}^2$
g_G	Geothermal gradient, $^\circ\text{F/ft}$
H	Enthalpy, Btu/lbm
h	Productive interval depth, ft
k	Permeability of the productive interval, md
k_e	Formation thermal conductivity, $\text{Btu/hr.ft.}^\circ\text{F}$
J	Conversion factor, 778 ft.lbf/Btu
L	Length of flow string, ft
L_R	Relaxation length parameter given by Eq. 20, ft^{-1}
m	Mass of fluid per unit length, lbm/ft
Q	Rate of heat transfer, Btu/hr.ft.
r	radial coordinate
r_{cem}	Cement radius, ft

r_{ci}	Inside casing radius, ft
r_{co}	Outside casing radius, ft
r_{ins}	Insulation radius, ft
r_{ti}	Inside tubing radius, ft
r_{to}	Outside tubing radius, ft
s	skin, dimensionless
t	Production time, hr
t_D	Dimensionless time
T_D	Dimensionless temperature
T_{ei}	Undisturbed formation temperature at any depth, °F
T_{eibh}	Undisturbed formation temperature at bottomhole, °F
T_{eij}	Undisturbed formation temperature at previous depth, °F
T_f	Tubing fluid temperature, °F
T_{fi}	Initial tubing fluid temperature at the start of time step, °F
T_{fj}	Tubing fluid temperature at previous depth, °F
T_{fws}	Tubing fluid temperature without superposition, °F
T_{wb}	Temperature at the wellbore/formation interface, °F
U	Overall heat transfer coefficient, Btu/hr.ft ² .°F
v	Velocity of fluid, ft/hr
w	Mass flow rate of tubing fluid, lbm/hr
x	Weights assigned to particular depths, dimensionless
z	Well depth, ft

z_j	Well depth at the previous step, ft
α	Wellbore inclination with horizontal, degrees
α_e	Thermal diffusivity of formation, ft ² /hr
ξ	Lumped parameter defined by Eq. 25, °F/ft
ϕ	Lumped parameter defined by Eq. 2, °F/ft
ψ	Lumped parameter defined by Eq. 28, °F/ft

TABLE OF CONTENTS

	Page
ABSTRACT	ii
DEDICATION	iv
ACKNOWLEDGEMENTS	v
NOMENCLATURE	vii
TABLE OF CONTENTS	x
LIST OF FIGURES	xii
LIST OF TABLES	xiv
CHAPTER I INTRODUCTION	1
CHAPTER II LITERATURE REVIEW	6
Steady-state and Transient Modeling	6
Inverse Modeling and Distributed Temperature Sensing (DTS)	9
Near Wellbore and Well Cleanup	10
CHAPTER III MODEL DEVELOPMENT	12
Introduction	12
Steady-state Model	13
Transient Model	15
Effect of Varying Heat Flux on Heat Transfer	16
Steady-state Model	16
Transient Model	21
Inverse Modeling	22
Summary	25
CHAPTER IV MODEL APPLICATION	26
Introduction	26
Steady-state Modeling	28
Well 2	28

Well 3	32
Transient Modeling	35
Well 2	39
Well 3	41
Well 4	42
Summary	47
 CHAPTER V FIELD APPLICATION	 48
Introduction	48
Estimating Reliable Rates with Temperature Modeling	49
Cleanup Effect in Pressure-Transient Response	52
Summary	58
 CHAPTER VI DISCUSSION AND CONCLUSION	 59
 REFERENCES	 62
 APPENDIX A PRESSURE DATA	 70
 APPENDIX B SAMPLE CALCULATION	 73

LIST OF FIGURES

	Page
Figure 1 – General well configuration involving a variety of elements.....	14
Figure 2 – Schematic representation of superposition principle.	18
Figure 3 – Depth dependent measurement of transient temperature in Well 3.....	27
Figure 4 – History matching temperature profiles at various rates for Well 2.....	30
Figure 5 – History matching temperature profiles at various depths for Well 2.....	31
Figure 6 – History matching temperature profiles at various rates for Well 3.....	33
Figure 7 – History matching temperature profiles at various depths for Well 3.....	34
Figure 8 – Depth-dependent measurements of transient temperature in Well 4.	36
Figure 9 – Gas Rate and Fluid Temperature during the cleaning phase in Well 4.	38
Figure 10 – History matching transient temperature profile, Well 2.	40
Figure 11 – History matching transient temperature profile, Well 3.	41
Figure 12 – History matching transient temperatures profile, Well 4.....	42
Figure 13 – History matching transient temperature profiles using data at different depths, Well 4.	44
Figure 14 – Estimated rate profile using temperature data at different depths, Well 4. ..	45
Figure 15 – History matching transient temperature profile using data nearest to the mudline, Well 4.....	46
Figure 16 – Estimated rate profile using temperature data nearest to the mudline, Well 4.....	47
Figure 17 – Temperature history matching using transient and steady-state models for cleanup phase, Well 4.	50
Figure 18 – Comparison of measured and estimated rates during the cleanup phase, Well 4.....	50

Figure 19 – Temperature estimation at different depths with and without superposition for cleanup phase, Well 4.....	51
Figure 20 – Pressure simulation for one of the design cases.	53
Figure 21 – Rate simulation for the same case as Fig. 20.....	54
Figure 22 – Buildup charts for the same case as in Fig. 10.....	54
Figure 23 – Pareto chart showing the significance of independent variables in skin from BU-1.....	56
Figure 24 – Pareto chart showing the significance of independent variables in skin from BU-2.....	56
Figure 25 – Incomplete cleanup manifests in terms of skin, Well 4.....	57

LIST OF TABLES

	Page
Table 1 – Input parameters for Well 2.	29
Table 2 – Error estimation in computed rates, Well 2.	31
Table 3 – Input parameters for Well 3.	32
Table 4 – Error estimation in computed rates, Well 3.	35
Table 5 – Input parameters for Well 4.	43
Table 6 – Design variables for full factorial analysis.....	55

CHAPTER I

INTRODUCTION

One of the wonders of modern science is the ability to discover or create energy intensive fuels. The on-going battle between the depleting energy resources and the initiatives to find new ones has given birth to a need of a greater workforce striving towards this important task. According to recent surveys, the World population is expected to increase by a billion in the next decade. Due to such unprecedented increase in population, energy demands are expected to soar high as well. And with most of the 'easy hydrocarbon' almost on the verge of depletion, it behooves us to remember that the total hydrocarbon reserve of the world is finite and it is dwindling every day. Thus it becomes incumbent to find new resources and develop efficient and economically feasible means of extracting the available ones.

Oil and gas bearing pay zones are porous rock media that are found thousands of feet below the earth's surface. At such depth the fluids possess energy in the form of high pressure and temperature. Wells are drilled to produce these fluids from these pay zones. In producing these fluids, the engineers have to contend with two major types of energy loss. Energy is lost from the fluid in moving from the porous medium to the wellbore and then moving from the well bottom, henceforth called bottomhole, to the wellhead. This study provides models that deal mostly with the latter.

A reservoir's potential is determined by its ability to economically produce the fluids present in the porous medium. This ability depends on both the properties of the reservoir fluids and the properties of the porous rock medium. To gauge this potential, oil companies in the United States and all over the world spend millions of dollars a year in well testing to estimate parameters related to these factors. In order to estimate useful properties from the testing, the transient bottomhole pressure response along with the surface or bottomhole rate measurements are required for any analysis. Pressure measurements are often reliably available with a reasonable degree of accuracy. Rate measurements, on the other hand, often lack synergy with pressure due to sensor resolution and/or frequency of monitoring. Such measurements may introduce significant uncertainty in transient tests interpretations. Furthermore in deep reservoirs where temperatures and pressures are high, failure of measuring gauges add to the cost and uncertainty of a test.

Accurate heat transfer modeling can contribute significantly in that realm. Earth temperature generally increases with depth. Thus, as the hot fluid from bottomhole rises up the wellbore, its temperature is higher than the surrounding Earth temperature which causes it to lose heat to the surroundings. When the flow rate of the fluid increases, more of the hotter fluid from the bottom displaces the colder fluid in the wellbore at any given point and therefore the temperature increases. Conversely, with a drop in fluid rate, the rate of displacement is going to decrease, thus bringing about a decrease in the rate of temperature increment. Hence, it is observed that temperature profiles tend to follow rate

profiles to a great extent for at least low to moderately high flow rates. Investigation of such a relationship to compute rates and fill the gap where rate measurements are lacking or doubtful require sound inverse modeling of flowing wellbore fluid temperature.

Perhaps the most common form of transient testing is the flow-after-flow test. Such tests usually consist of stabilized flow periods. Even if the flow period is still transient, more often than not the flow duration causes the thermal transients to settle and steady state to kick in. During such a time, the inverse modeling requires a steady-state model to predict temperature and subsequently estimate rate. Moreover in drillstem testing, analyses of transient data are generally restricted to that of post-cleanup period because rates often go unmonitored at early times during the cleanup phase, unless aided by multiphase flow metering. The value of early-time production data monitoring may be overlooked for two reasons: first, transients may be difficult to interpret because of two-phase flow in the formation; second, two-phase flow metering becomes a requirement. Such a void necessitates the application of a more rigorous transient analytical model to apply the mentioned approach. Estimation of flow rates for the cleanup period would facilitate their use in transient analysis. Intrinsicly, if reasonable formation conductivity (kh) and skin can be extracted from the cleanup period, considerable time saving can result because the designed test sequence can be altered with respect to flow rates and flow periods commensurate with test objectives.

A great deal of work has been done in the field of heat transfer in wellbores. Lesem et al. (1957), Ramey (1962), Willhite (1967) and Alves et al. (1992) have all made significant contributions to the field. However nearly all flowing fluid temperature models assume that heat exchange between the formation and the fluid remains constant throughout the entire production time. Hasan and Kabir (1994) and Hasan et al. (2005) have developed steady state and transient models for estimating fluid temperature. These models too assume constant flux between the wellbore and the formation at their core.

In this work, we have undertaken the task of developing a model to account for the variable flux between the wellbore and the formation. With proper forward modeling of heat transfer, temperature measurements can serve some really useful purposes. Coupling multiple temperature measurements to help with interpretation can provide further usefulness. These are more commonly known as distributed temperature measurements where the fluid temperature measurement is made at several depths along the wellbore. We use the superposition model in conjunction with the established steady-state and transient temperature models for the inverse modeling of temperature to estimate flow rates.

In the next chapter, we discuss the available literature on the forward modeling of flowing fluid temperature profile in wellbores and the inverse modeling phenomenon. In the first part of the chapter, the focus is on thermal flow modeling and estimation of flow rate from temperature measurements. Various applications of distributed-temperature

sensing (DTS) are also mentioned. The second part of the chapter emphasizes on the near-wellbore issues and the investigation of the cleanup period.

In Chapter III, we demonstrate the model development for the superposition of heat flow and the approach involving the use of the steady-state and the transient models to estimate flow rate. Chapter IV presents case studies where the estimations and the predictions are compared against field data supplied by Hess Corporation. A discussion of the application and simulated examples that probe the possibility of extracting meaningful information from the cleanup data are highlighted in Chapter V. Chapter VI finally presents conclusions and some recommendations.

CHAPTER II

LITERATURE REVIEW

Production of gas and oil constitutes significant heat transfer between the wellbore fluid and the formation. This is due to the fact that the rising fluid in the wellbore is generally at a much higher temperature than the surrounding wellbore which sets a temperature differential conducive to heat loss from the fluid. The modeling of this heat transfer becomes a more involved process as the exchange depends on both time duration of the flow and the position in the wellbore. The modeling is significant since most of the fluid properties are a function of temperature. Hence for accurate pressure profiling, needed for gauging vertical flow performance or determining choice of materials for facilities and equipment design, fluid temperature needs to be known. In this study, we have reviewed previous work involving steady-state and transient heat transfer modeling along with application of data from distributed temperature sensing (DTS). One of the applications of DTS, that has been discussed, is the estimation of fluid flow rate from temperature data for the cleanup period of a newly drilled well. We comment on some of the work done with regards to the investigation of the cleanup period.

Steady-state and Transient Modeling

One of the earliest works in this field could be traced back to Schlumberger et al. (1937) who pointed out the usefulness of measuring wellbore fluid temperature. Following this, there were a few developments in the area but it was not until two decades later that

Lesem et al. (1957) and Moss and White (1959) came up with procedures to estimate wellbore fluid temperature. However Ramey (1962) and Edwardson et al. (1962) were the first ones to present a theoretical model to estimate fluid temperature as a function of well depth and production time. Following these classical works, many researchers such as Willhite (1967), Pacheco and Farouq Ali (1972), Herrera et al. (1978), Hong and Griston (1986) and Willhite and Griston (1987) used Ramey's model in various applications. However these models neglected kinetic and frictional energy losses in their development and were limited to single-phase fluids only. In addition to that, the models made use of the line source assumption and treated the wellbore radius to be negligible. While these assumptions may work in steady-state cases, they cause significant inaccuracy during early times. Several improvements of these models have been suggested since. Satter (1965) improved on Ramey's work by including the effects of phase change in his modeling with steam injection wells. Shiu and Beggs (1980) proposed a method for estimating a specific parameter in Ramey's equation. Sagar et al. (1991) made a significant improvement by extending Ramey's work to include multiphase flow and accounting for kinetic energy effects and Joule-Thompson expansion using an empirical approach. Alves et al. (1992) came up with a unified equation for flowing temperatures which was applicable to both pipelines and wellbores, and degenerated into Ramey's equation for single phase incompressible liquid. Hasan and Kabir (1994) improved on the line source assumption by appropriating the wellbore as a cylindrical source. In addition, they also accounted for convective heat transfer in the casing annulus, demonstrating excellent coherence with the field data. In more recent

time, Hagoort (2004) illustrated a graphical correlation to estimate the length of early transient period of flowing well. This development was based on the result of revisiting Ramey's model on which Hagoort (2005) made further improvement by presenting an analytical solution for wellbore fluid temperature of gas wells.

Since then more focus has been given to forward modeling of transient temperatures in wellbores especially in terms of transient testing. Some of the early notable works involve Kabir et al. (1996) and Fan et al. (2000). Hasan et al. (2005) developed analytical models for transient wellbore fluid temperature for both draw-down and build-up for transient gas-well testing. Their models were validated with field data. Guo et al. (2006) also designed a model for estimating temperature profiles in pipelines with different kinds of insulations. Their model assumed conduction to be the only mode of significant heat transfer. Izgec et al. (2007) proposed improvements to the previous analytic temperature models by developing a numerical differentiation scheme which removed the limitations imposed by the constant relaxation parameter assumption used in previous models. In a more recent study, Bahonar et al. (2011 a, b) developed a numerical fully implicit non-isothermal wellbore/reservoir simulator. They solve the heat transfer problem in much the same way as Hasan et al. (2005) and stretch its application to the design of gas well tests and interpretation of both isothermal and non-isothermal gas reservoirs.

Inverse Modeling and Distributed Temperature Sensing (DTS)

The dependence of fluid temperature on flow rate can be used inversely to estimate rate given temperature data. Inverse modeling has also become possible with the availability of such robust models and high speed computing in today's age. The idea of inverse modeling is not new. Witterholt and Tixier (1972) and Curtis and Witterholt (1973) first used the influence of flow rate on fluid temperature in Ramey's equation in conjunction with measured temperature, for qualitative estimation of flow rate from various producing zones. Their method could not work for estimating flow rates from multiple zones, largely owing to the dependence of the method on the establishment of constant temperature difference between the wellbore fluid and formation. Since the time of Curtis and Witterholt, inverse modeling has been studied by many researchers. Kabir and Hasan (1998) and Izgec et al. (2009) explored the different issues with inverse modeling in terms of the placement of gauges. The more recent successes though that inverse modeling has seen are in terms of distributed temperature measurements.

DTS has shown tremendous potential with various forms of testing and analysis. The approach can also be extended to help with drillstem testing. Most often for drillstem testing, pressure and temperature measurements are made at the wellhead and bottomhole. DTS data in this context is rarely reported, although DTS is quite prevalent in permanent completions nowadays. Numerous studies have been done on DTS and various applications are discussed in literature. Some of these applications include matrix treatment diagnosis (Glasbergen et al. 2009, 2010; Tan et al. 2012), zonal

contribution assessment (Tardy et al. 2012, Parta et al. 2010), fracture-stimulation diagnosis (Tabatabaei et al. 2012), and injection profiling (Gao et al. 2008, Hoang et al. 2012), among others. Duru and Horne (2010) made use of DTS data for estimating formation parameters, such as permeability and porosity, among others, during transient testing.

Wang et al. (2008) presented a flow-profiling inverse model using DTS technology. The model is applicable for both gas and oil but is based on steady-state energy balance. Kabir et al. (2012) built further on the Wang et al. (2008) model by combining it with flow rate estimation methods proposed by Izgec et al. (2010). The combination facilitated the estimation of the entire suite of flow information, independent of wellhead flow measurements. However Izgec et al. (2010) model used a constant to account for Joule-Thompson and the kinetic energy effects.

Near Wellbore and Well Cleanup

Applicability of fluid temperature data in transient testing can also be extended to the near wellbore region. As discussed earlier, temperature measurements provide a unique opportunity to estimate flow rates. This can be extremely useful in areas where rate information is not available. Subsequently, the rates can be used in transient analysis. Such a technique could be used for the analysis of the cleanup period where the rates are normally not metered due to variable multiphase flow. Important parameters can be obtained this way when near wellbore damage precludes use of cleanup data for

conventional testing. Since the near-wellbore properties are altered by the drilling operation itself, and the invasion of mud during over-balanced drilling, near-wellbore formation damage has been studied by investigators from various perspectives over the years. From the standpoint of transient-pressure testing, analysis of cleanup data was investigated by Larsen and Kviljo (1990) and Larsen et al. (1990). In these studies, the authors explored the variable-skin concept *en route* to establishing the attainment of cleanup. They showed with field data that the derived skin declines in a hyperbolic fashion in conventional tests. Stated differently, production of the invaded mud filtrate declines hyperbolically. This finding has considerable merit in that the diminishing influence of the unwanted phase with time was learned.

Systematic studies have also evolved in understanding variable skin in wireline-formation testing, wherein similar tests are run, but at a much reduced scale of producing rate and time. Studies of Goode and Thambynayagam (1996), Alpak et al. (2008), Ramaswami et al. (2012), among others, are cases in point. As expected, declining skin turned out to be the norm. Skin evolution has also been observed by Clarkson et al. (2013) in coal-bed methane wells. They coined the term dynamic-skin ratio, which was included in the dimensionless type-curve variables and flowing-material-balance formulation to include the effect of changing skin. More recently, Theuveny et al. (2013) explored various nuances of near-wellbore and wellbore cleanup operation with a transient multiphase wellbore simulator coupled with a reservoir-flow simulator.

CHAPTER III

MODEL DEVELOPMENT

Introduction

This chapter talks about the two flowing-fluid temperature modeling techniques, steady-state and transient that were developed by Hasan and Kabir (1994) and Hasan et al. (2005) respectively. Temperature models for wellbore fluid are developed using an energy balance between the wellbore fluid and its surrounding. Such an energy balance requires formation temperature distribution and overall heat transfer coefficient for the wellbore elements. When a well has been flowing at a constant rate for a relatively long period of time, the flow rate stabilizes and flowing temperature profile tends to reach a plateau. The temperature value at this plateau can be predicted using the steady-state model presented. Relatively easier implementation of steady-state model over the transient model provides the advantage of using it in cases where transient modeling is not essential. Conversely, transient modeling is more robust in terms of accounting time duration of production. When production is initiated or when the production rate is changed, thermal transients set in and take a much longer time to stabilize than their pressure counterparts. Generally speaking, the flow rate becomes stable soon after its initiation or change from one rate to another. However temperature changes for the corresponding period take much longer time to attain stability.

Improvement in both models has been suggested through the use of superposition of heat flow. Superposition principle here takes account for the variable heat flux between the wellbore and the formation. Inverse modeling is also explained later in the chapter. This forms an important section as it explains the basis and methodology of rate estimation using temperature.

Steady-state Model

Hasan and Kabir (1994) solved the thermal diffusivity equation for formation temperature using a wellbore of a finite radius. The basis of the analysis is that the steady-state heat flow from the tubing fluid to the wellbore/formation interface equals the heat flow from this interface to the formation. The heat flow from the tubing to the formation was modeled using an overall heat transfer coefficient which included thermal resistances for conduction and convection in the tubing, conduction through the tubing, insulation, casing and cement material. The flow of heat through the various layers can be more clearly understood by referring to the schematic from Hasan and Kabir (1994), shown in **Figure 1**. Natural convection in the annulus was also accounted for in their model. They developed the following linear differential equation to estimate the flowing fluid temperature in a wellbore for a steady-state system.

$$\frac{dT_f}{dz} = \frac{T_{ei} - T_f}{A} - \frac{g \sin \alpha}{c_p J g_c} + \phi \quad (1)$$

where

$$\phi = C_J \frac{dp}{dz} - \frac{v dv}{c_p J g_c} \quad (2)$$

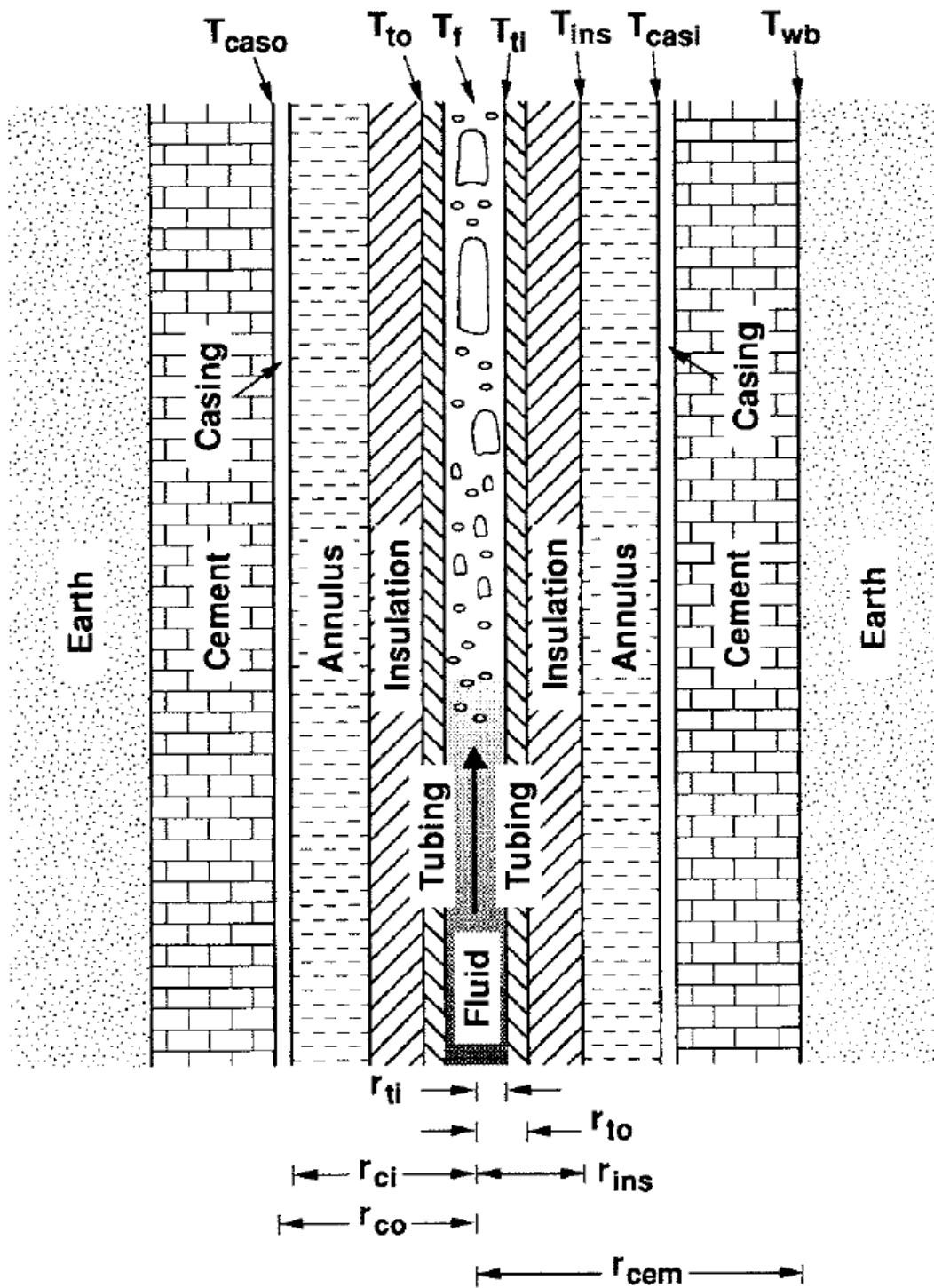


Figure 1 – General well configuration involving a variety of elements.

Goal of this chapter is to improve on this model by accounting for superposition. Moreover, the intent is to use the model in inverse modeling in order to estimate fluid rates in the well.

Transient Model

Modeling transient heat transfer for flowing fluid is usually complicated by the coupled nature of the three transport processes – heat, fluid, and momentum transports. Hasan et al. (2005) side-stepped this issue by assuming, based on their experience, that mass and momentum transport attains steady-state orders of magnitude faster than does heat transport. They also assumed that the change in temperature of the tubing/casing/cement material is proportional to that of the fluid and can be represented by the concept of thermal storage. This storage was represented in the form of a constant, C_T . Hasan et al. (2005) assumed a value of 3 for C_T for the drawdown period. In this study, it was discovered that the value of C_T is not constant and varies, perhaps depending on the material of the completions and time for which the well has been producing. This idea was not pursued though, and a different constant value was used for the case studies in the next chapter. The following expression for the transient temperature profile, developed by Hasan et al., is used in this work.

$$(1 + C_T) \frac{\partial T_f}{\partial t} - \frac{w}{m} \frac{\partial T_f}{\partial z} = \frac{w}{m} L_R [T_{ei}(z) - T_f] + \frac{w}{m} \left(\phi - \frac{g \sin \alpha}{c_p J g_c} \right) \quad (3)$$

Details of the two models are provided in each of the respective works. Both these models assume a constant heat flux between the fluid and the formation and therefore we present the concept of superposition in the next section.

Effect of Varying Heat Flux on Heat Transfer

In order to estimate the fluid temperature more accurately it is essential to incorporate changes that will account for the variation of heat flux with production time. We develop the concept of varying heat flux as following.

Steady-state Model

The rate of heat transfer, Q , from the wellbore to the formation (or vice versa) at the formation/wellbore interface per unit depth of the well (Btu/hr./ft.) is given by

$$Q = -\frac{2\pi k_e}{T_D(t_D)}(T_f - T_{ei}) \quad (4)$$

In Eq. 4, we assume the geothermal gradient to be linear with depth, i.e.,

$$T_{ei} = T_{eibh} - g_G(L - z) \quad (5)$$

The dimensionless temperature, $T_D(t_D)$, is a function of dimensionless time,

$$t_D = \frac{\alpha_e t}{r^2} \quad (6)$$

and can be estimated from (Hasan and Kabir, 2002),

$$T_D = \ln[e^{-0.2t_D} + (1.5 - 0.3719e^{-0.2t_D})\sqrt{t_D}] \quad (7)$$

However, Eq. 4 is only valid for constant heat flux at the wellbore/formation interface. In general, wellbore fluid temperature tends to approach the temperature of the formation

surrounding it, thereby decreasing heat transfer rate with time. To account for this changing heat flux we use the superposition principle. Let's consider a new well that has produced fluids at a constant rate for a time t . To estimate fluid temperature at time t , we divide the total into n periods (not necessarily equal) - $(t_1 - 0)$, $(t_2 - t_1)$, $(t_3 - t_2)$, ..., $(t_{n-1} - t_n)$ as shown in **Figure 2**. We assume that the heat flux at each of these time periods is constant.

Thus, at the first time step,

$$Q_1 = -\frac{2\pi k_e}{T_D(t_D)}(T_{wb} - T_{ei})_1 \quad (8)$$

Or,

$$T_{ei} - T_{wb,1} = \frac{Q_1 T_D(t_{Dn})}{2\pi k_e} \quad (9)$$

The heat flow rate, Q_2 , during the second time step, $t_2 - t_1$, will be different from Q_1 . This situation will be represented by adding another constant heat source, which supply heat to the well at time $> t_1$ and whose magnitude is equal to $Q_2 - Q_1$. The wellbore/formation interface temperature at this step, $T_{wb,2}$, is then the sum of the effects of these two heat sources and is given by,

$$T_{ei} - T_{wb,2} = \frac{Q_1 T_D(t_{Dn}) + (Q_2 - Q_1) T_D(t_{D,n} - t_{D1})}{2\pi k_e} \quad (10)$$

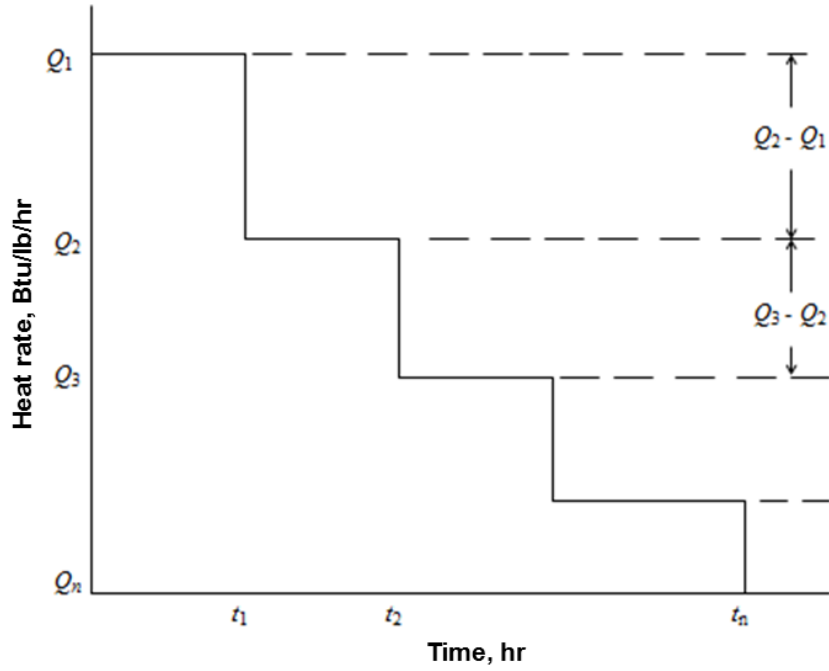


Figure 2 – Schematic representation of superposition principle.

Similarly, the third time period can be represented by three sources of heat supplying Q_1 from zero time, $Q_2 - Q_1$ since t_1 , and $Q_3 - Q_2$, since t_2 . Hence,

$$\begin{aligned}
 T_{ei} - T_{wb,3} & \\
 &= \frac{Q_1 T_D(t_{Dn}) + (Q_2 - Q_1) T_D(t_{Dn} - t_{D1}) + (Q_3 - Q_2) T_D(t_{Dn} - t_{D2})}{2\pi k_e} \quad (11)
 \end{aligned}$$

Hence for the n^{th} time period,

$$T_{ei} - T_{wb,n} = \frac{\sum_n}{2\pi k_e} \quad (12)$$

where

$$\sum_n = \sum_{i=1}^n (Q_i - Q_{i-1}) T_D(t_{Dn} - t_{D,i-1}) \quad (13)$$

and both Q_0 and T_{D0} are zero.

The flowing wellbore fluid temperature is obtained from an energy balance between the wellbore fluid and the surrounding formation at the time of interest, t . The rate of heat transfer from the wellbore fluid to the wellbore/formation interface, in terms of the overall heat transfer coefficient for the wellbore, is given by,

$$Q_n = -2\pi r U (T_f - T_{wb})_n \quad (14)$$

Hence,

$$T_{wb,n} = T_{f,n} + \frac{Q_n}{2\pi r U} \quad (15)$$

Substituting this expression for $T_{wb,n}$ into Eq. 12, we get

$$T_{ei} - T_{f,n} = \frac{Q_n}{2\pi r U} + \frac{(Q_n - Q_{n-1})T_D(t_{D,n} - t_{D,n-1})}{2\pi k_e} + \frac{\Sigma_{n-1}}{2\pi k_e} \quad (16)$$

where Σ_{n-1} is defined the same way as Eq. 13 for $n-1$ elements. Or

$$T_{ei} - T_{f,n} = \frac{Q_n}{2\pi} \left[\frac{1}{rU} + \frac{T_D(t_{D,n} - t_{D,n-1})}{k_e} \right] - \frac{(Q_{n-1})T_D(t_{D,n} - t_{D,n-1})}{2\pi k_e} + \frac{\Sigma_{n-1}}{2\pi k_e} \quad (17)$$

Rewriting Eq. 17 in a different form, we get

$$T_{ei} - T_{f,n} = \frac{Q_n}{2\pi} \left[\frac{k_e + rUT_D(t_{D,n} - t_{D,n-1})}{rUk_e} \right] - \frac{(Q_{n-1})T_D(t_{D,n} - t_{D,n-1})}{2\pi k_e} + \frac{\Sigma_{n-1}}{2\pi k_e} \quad (18)$$

and thus for Q_n ,

$$Q_n = wc_p L_{R,n} (T_{ei} - T_{f,n}) + \frac{T_D (t_{D,n} - t_{D,n-1}) (B_n Q_{n-1})}{k_e} - \frac{B_n \Sigma_{n-1}}{k_e} \quad (19)$$

where

$$L_R = \frac{2\pi}{c_p w} \left[\frac{r U k_e}{k_e + r U T_D (t_{D,n} - t_{D,n-1})} \right] \quad (20)$$

and

$$B_n = \frac{r U k_e}{k_e + r U T_D (t_{D,n} - t_{D,n-1})} = \frac{w c_p L_R}{2\pi} \quad (21)$$

Energy balance on the flowing fluid for a differential depth, dz , gives,

$$\frac{dT_f}{dz} = \frac{1}{c_p} \left[-\frac{Q_n}{w} - \frac{g \sin \alpha}{g_c J} - \frac{v}{g_c J} \frac{dv}{dz} \right] + C_J \frac{dp}{dz} \quad (22)$$

Substituting the expression for Q_n from Eq. 19 into Eq. 22, we obtain

$$\begin{aligned} \frac{dT_f}{dz} = & -L_{R,n} (T_{ei} - T_{f,n}) - \frac{g \sin \alpha}{g_c J c_p} - \frac{v}{g_c J c_p} \frac{dv}{dz} + C_J \frac{dp}{dz} \\ & - \frac{T_D (t_{D,n} - t_{D,n-1}) (L_{Rn} Q_{n-1})}{2\pi k_e} + \frac{L_{Rn} \Sigma_{n-1}}{2\pi k_e} \end{aligned} \quad (23)$$

Or

$$\frac{dT_{f,n}}{dz} = -L_R T_{ei} + L_R (T_{f,n}) - \frac{g \sin \alpha}{g_c J c_p} + \phi + \xi \quad (24)$$

where

$$\xi = -\frac{T_D (t_{D,n} - t_{D,n-1}) (L_{Rn} Q_{n-1})}{2\pi k_e} + \frac{L_{Rn} \Sigma_{n-1}}{2\pi k_e} \quad (25)$$

and

$$\phi = C_J \frac{dp}{dz} - \frac{v dv}{c_p J g_c} \quad (2)$$

We can then rewrite Eq. 24 as,

$$\frac{dT_{f,n}}{dz} = \frac{dT_{fws}}{dz} + \xi \quad (26)$$

where T_{fws} is the fluid temperature estimated without superposition. Assuming that ξ is invariant, the linear differential equation, Eq. 26 is solved as

$$T_f = T_{ei} + \frac{(1 - e^{(z-L)L_R})}{L_R} (\psi + \xi) \quad (27)$$

where

$$\psi = g_g \sin\alpha + \phi - \frac{g \sin\alpha}{g_c J c_p} \quad (28)$$

Transient Model

Eq. 27 provides the temperature equation with superposition for the steady state model. The transient model can be developed with the similar principles using the transient differential equation. For this analysis, we assume that fluid flow transients subside quickly and that flow rate, w , is independent of well depth. An energy balance indicates that any heat received/lost from the formation would change the fluid temperature with time and depth. In terms of fluid internal energy fluid enthalpy H , fluid mass rate w , fluid mass in the control volume m , the energy balance equation can be expressed as

$$Q = \frac{d}{dt} [m c_p T_f (1 + C_T)] - \frac{d}{dz} \left[w \left(H + \frac{1}{2} v^2 - g z \sin\theta \right) \right] \quad (29)$$

The term C_T , represents the heat storage effect of the tubulars and cement sheaths in the wellbore. The heat received from (or lost to) the formation, Q , is given by Eq. 8

$$Q_1 = -\frac{2\pi k_e}{T_D(t_D)}(T_{wb} - T_{ei})_1 \quad (8)$$

As we discussed in the previous subsection, the requirement of a constant Q can be allowed for by subdividing the time in consideration into discrete temporal steps. Analogous to the derivation of Eq. 24, we obtain the following differential equation for fluid temperature as a function of time and depth,

$$\frac{dT_f}{dz} = \frac{wc_p L_R}{mc_p(1 + C_T)}(T_{ei} - T_f) + \frac{wc_p}{mc_p(1 + C_T)}(1 - e^{(z-L)L_R})(\psi + \xi) \quad (30)$$

Again, assuming ξ and ψ to be constant, we arrive at the following expression for fluid temperature,

$$T_f = T_{ei} + (T_{fi} - T_{ei})e^{-at} + \frac{(1 - e^{-at})}{L_R}(1 - e^{(z-L)L_R})(\psi + \xi) \quad (31)$$

Where

$$a = \frac{wc_p L_R}{mc_p(1 + C_T)} \quad (32)$$

In many situations, the differences in prediction when using Eq. 24 and Eq. 30 as opposed to Eq. 1 and Eq. 3 are not large. Thus, while less accurate, using Eq. 1 and Eq. 3, in cases where ξ is not large, for the sake of simplicity and saving computation time, may be acceptable.

Inverse Modeling

During production, fluid temperature at various depths in the wellbore can be estimated using the fluid rate as shown in the previous sections. When the distributed temperatures are available, the opportunity arises to solve the inverse problem for estimating rates.

Using the boundary conditions as shown by Hasan et al. (2009), the following model can be derived from Eq. 1 for a depth-by-depth estimation of temperature.,

$$T_f = T_{ei} + \frac{(1 - e^{(z-z_j)L_R})}{L_R}(\psi + \xi) + e^{(z-z_j)L_R}(T_{fj} - T_{eij}) \quad (33)$$

where L_R is defined in a similar manner as Eq. 20. As shown by Eq. 33 and Eq. 20, the fluid temperature depends on L_R , which in turn depends on the mass flow rate, w . This relationship between the fluid temperature and the mass flow rate forms the basis of the computational approach suggested. The approach was also outlined in a recent study by Izgec et al. (2010). However the non-linear relationship between the fluid temperature and rate does not lend itself for a direct solution of rate from fluid temperature. This is why we use an iterative procedure. The process involves guessing a rate, followed by calculating the fluid temperature throughout the wellbore using Eq. 33. The calculated temperature, T_c , is then compared with the known fluid temperature, T_{data} , at the depths of interest and the following optimization function minimized,

$$\sum x(T_c - T_{data})^2 \quad (34)$$

where x represents the weight that can be assigned to particular depths where the temperature data shows more fidelity or where more confidence in the data exists. Intuitively shallower depths would show more fidelity than deeper measurements. During the procedure, the magnitude and the direction of the error in temperature, $(T_c - T_{data})$, can be used to guess a better value of the rate. The multiple depths help reduce the uncertainty and non-uniqueness in the optimization. The process also allows optimization of those parameters which are often known with some degree of

uncertainties, such as cement conductivity, thermal conductivity of fluid and pipe roughness. Once optimization is done, the same parameters should be used throughout the entire process for any specific well. Application of this procedure is shown in the next chapter.

The process mentioned thus far is intended for steady-state modeling. Inversion with transient temperature modeling required a more complex and calculation-intensive algorithm. We divide the production time into several time-steps, not necessarily equal. It should be noted that there could be as many time steps as preferred by the user. The smaller the time intervals, the better the accuracy is for the estimated rates. In other words, with more number of time steps in the process, more accurate rates would be estimated.

Using initial and boundary conditions as defined below,

Boundary condition:

$$T_f(L, t) = T_{eibh} \quad (35)$$

Initial condition:

$$T_f(z, 0) = T_{eibh} - (L - z)g_G \sin\alpha \quad (36)$$

the following transient model can be obtained from Eq. 30,

$$T_{f,n} = T_{ei} + \frac{(1 - e^{-a(t_n - t_{n-1})})(1 - e^{(z-L)L_R})}{L_R} (\psi + \xi) + (T_{f,n-1} - T_{ei})e^{-a(t_n - t_{n-1})} \quad (37)$$

Temperature at the end of each time step is used as an initial condition for the following time step. This procedure, though more calculation intensive, allows for better granularity in the estimations and thus can be compared with data from metering at multiple different depths and times using Eq. 34. Once again, having data at different depths would help reduce the uncertainty and non-uniqueness in the estimation matrix.

Summary

Steady-state and transient modeling of flowing wellbore fluid temperature is highlighted with improvement suggested through the use of superposition of heat flow. Detailed modeling of heat flow superposition is shown for both steady-state and transient models. Inverse modeling is discussed with detailed description of the optimization procedure followed and the equations used.

The application of the models and techniques developed is shown in the next chapter for both steady-state and transient models with inverse modeling to estimate flow rates using field data.

CHAPTER IV

MODEL APPLICATION

Introduction

The last chapter talked about the details and the methodology that was adopted in the modeling of temperature and inverse modeling. Here we present some of the field cases where the model was applied. The data was supplied by Hess Corporation from their deepwater asset in Western Australia. In this setting, the mudline generally occurs around 3,500 ft, with productive intervals ranging from 10,000 to 17,000 ft. Temperature and rate data both were available for this study. For temperature data, the acoustic surface-readout technology was used by the operator which allowed for measurements from downhole gauges in real time. The acoustic units were installed onto the outside of the tubing string, approximately every 1500 ft below the mudline. The temperature sensors on these units had an accuracy of $\pm 1.5^{\circ}\text{C}$. The rates were measured using a multiphase flow meter. **Figure 3** presents a picture of the entire data set available for Well 3. Similar data sets were available for other wells which are discussed in the subsequent sections. Such distributed data set provides the feasibility of such modeling. Even in cases where distributed data is not present, as we show later, the technique can be made use of by utilizing just the wellhead information. However in that case, the user has to compromise on accuracy and uniqueness. This point is discussed later in this chapter.

The wells were initially flowed with increasing high rates as can be seen in Figure 3. This period is the cleanup period. After this, the well is shut-in for some time and then flowed again for the flow-after-flow test. In this test, the well is flowed at a constant flow rate till the flowing pressure achieves pseudo-steady state (PSS), at which point the rate is increased to another constant value till PSS is achieved again. This is repeated for a set of four or five rates.

We attempt to provide solutions for only the dry section of the well. This is because the uncertainty in the heat-transfer parameters in the wet section and convective heat loss at the wellhead, precipitated by variable wind speed and other factors, collectively demand a large entry of accurate information for credible solutions.

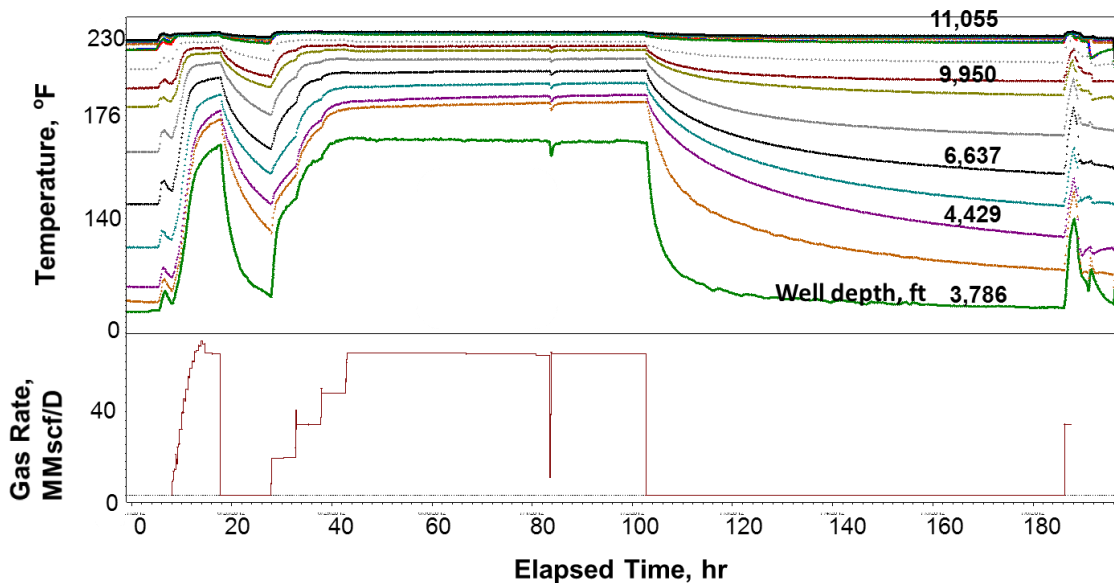


**Figure 3 – Depth dependent measurement of transient temperature in Well 3.
(Kabir et al. 2014)**

Steady-state Modeling

Two wells were studied for the steady-state modeling purpose. The match and the solutions later on are provided for the steady part of the flow during the flow-after-flow analysis. Computation starts with a known pressure and temperature at the bottomhole. Thereafter, temperature of the next segment is calculated using Eq. 33.

Well 2

The details of the input parameters used for Well 2 are presented in **Table 1**. Using these inputs, temperature profiles were generated at different rates for the flow after flow analysis.

Total Vertical Depth, ft	9,032
Measured Depth, ft	10,194
Inclination below 7,000 ft, degrees	52
Pipe Roughness, ft	0.000465
Tubing ID, in.	3 4/5
Tubing OD, in.	6
Casing ID, in.	8 15/22
Casing OD, in.	9 5/8
Cement ID, in.	9 5/8
Cement OD, in.	12
Mudline Temperature, °F	50
Bottomhole Temperature, °F	182
Coefficient of Thermal Expansion (β), 1/°F	0.00011
Critical Pressure, psia	671.14
Critical Temperature, °R	367.74
Specific gravity of gas	0.643
Thermal conductivity of tubing fluid, Btu/(hr-ft-°F)	0.018
Thermal conductivity of tubing and casing, Btu/(hr-ft-°F)	26
Thermal conductivity of annulus fluid, Btu/(hr-ft-°F)	0.4
Thermal conductivity of cement, Btu/(hr-ft-°F)	0.6
Thermal conductivity of formation, Btu/(hr-ft-°F)	1.4
Specific heat of gas, Btu/(lbm-°F)	0.78
Specific heat of annular fluid, Btu/(lbm-°F)	1
Density of annular fluid, lbm/ft ³	67.15
Viscosity of annular fluid, cp	1
Geothermal gradient, °F/ft	0.0252

Table 1 – Input parameters for Well 2.

History matching of temperature profiles for various rates is shown in **Figure 4**. It should be noted that only one set of input parameters were used for the entire depth and time. The continuous lines, which represent the model estimations, compare well with the data points shown. **Figure 5** presents the inverse modeling efforts to generate the

steady-state rates based on the temperature match shown in Figure 4. Here the temperature is plotted against rates at various depths.

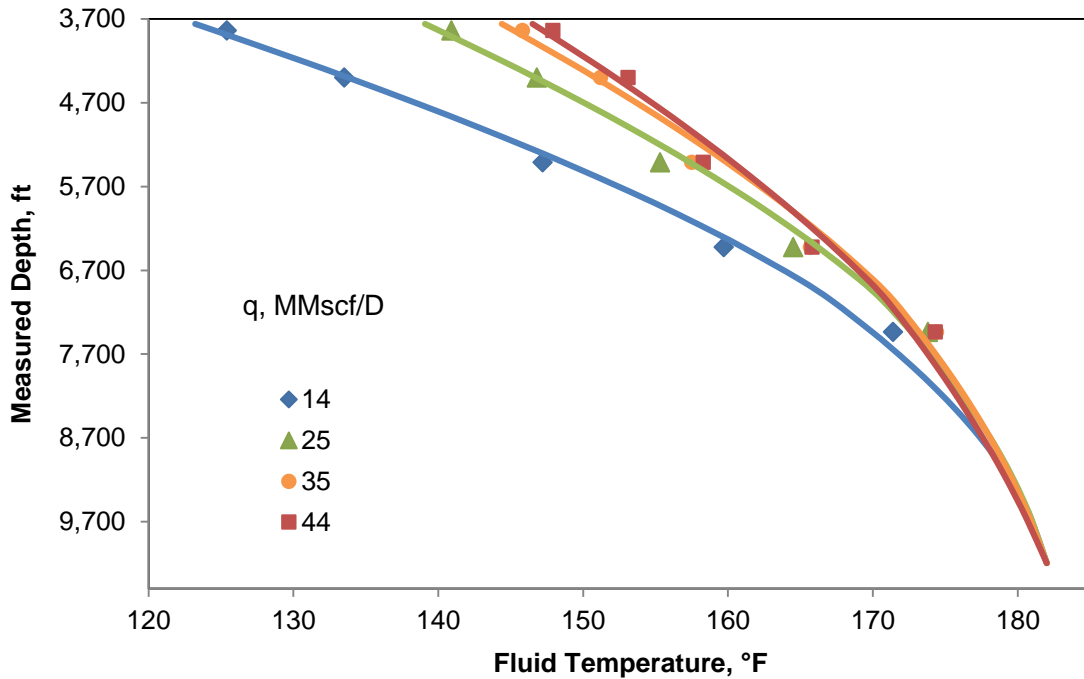


Figure 4 – History matching temperature profiles at various rates for Well 2. (Kabir et al. 2014)

As expected, the smallest response occurs as we move towards the bottom of the well. The largest excursion is seen near the mudline. Hence, as mentioned in Chapter III, more weightage can be assigned to the depths near the mudline for inverse modeling. In Figure 5, only the few more important depths are shown whereas Figure 3 shows that data was available for more stations. The gauges that made a difference to the rate estimation during inverse modeling are shown.

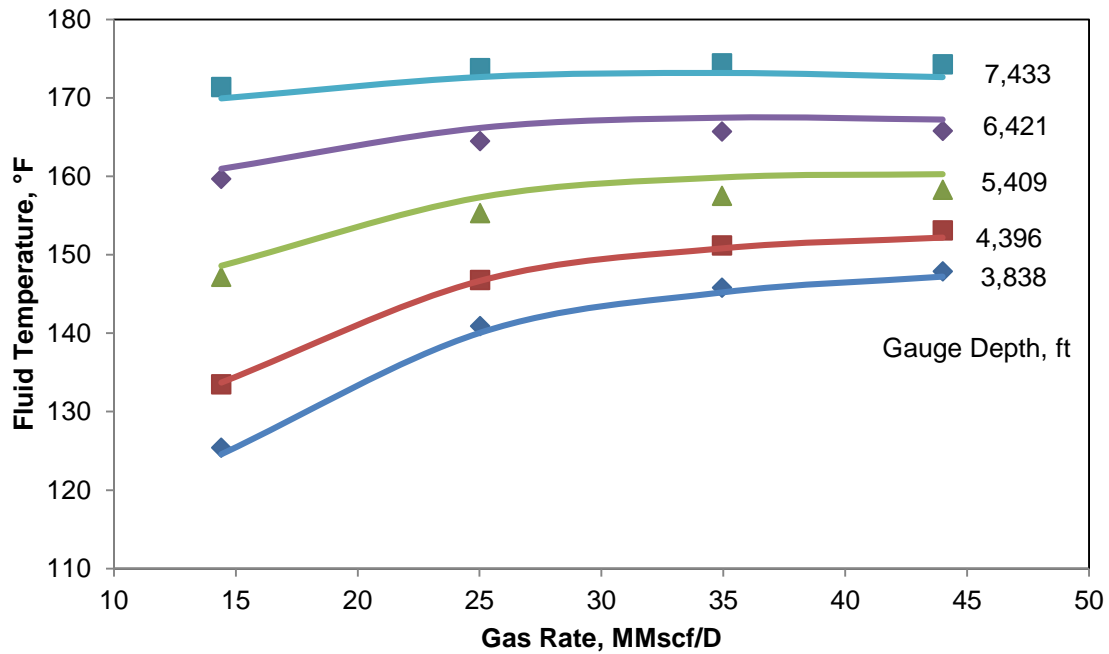


Figure 5 – History matching temperature profiles at various depths for Well 2. (Kabir et al. 2014)

Table 2 presents the error analysis of the rates that were obtained by matching the temperatures as shown in Figure 4 and Figure 5.

	Flow Rate, MMscf/D			
	Rate 1	Rate 2	Rate 3	Rate 4
Computed	14.87	25.04	33.17	49.68
Measured	14.40	25.02	34.95	44.00
Error (%)	3.29	0.07	-5.11	12.91

Table 2 – Error estimation in computed rates, Well 2. (Kabir et al. 2014)

As shown in Table 2, the rates predicted are within engineering accuracy.

Well 3

Table 3 presents the input parameters used for Well 3. A similar analysis was carried out for Well 3 as for Well 2.

Total Vertical Depth, ft	11,572
Measured Depth, ft	11,840
Inclination below 8,800 ft, degrees	28
Pipe Roughness, ft	0.00027
Tubing ID, in.	3 4/5
Tubing OD, in.	4.5
Casing ID, in.	8 15/22
Casing OD, in.	9 5/8
Cement ID, in.	9 5/8
Cement OD, in.	13
Mudline Temperature, °F	41
Bottomhole Temperature, °F	227.3
Coefficient of Thermal Expansion (β), 1/°F	0.00011
Critical Pressure, psia	671.14
Critical Temperature, °R	367.74
Specific gravity of gas	0.643
Thermal conductivity of tubing fluid, Btu/(hr-ft-°F)	0.011
Thermal conductivity of tubing and casing, Btu/(hr-ft-°F)	26
Thermal conductivity of annulus fluid, Btu/(hr-ft-°F)	0.4
Thermal conductivity of cement, Btu/(hr-ft-°F)	0.6
Thermal conductivity of formation, Btu/(hr-ft-°F)	1.4
Specific heat of gas, Btu/(lbm-°F)	0.78
Specific heat of annular fluid, Btu/(lbm-°F)	1
Density of annular fluid, lbm/ft ³	67.15
Viscosity of annular fluid, cp	0.6
Geothermal gradient, °F/ft	0.02322

Table 3 – Input parameters for Well 3.

History matching of temperature profiles for this case is shown in **Figure 6**. As shown before, the match was predicated upon honoring the last temperature data point, for a given flow rate, at each depth.

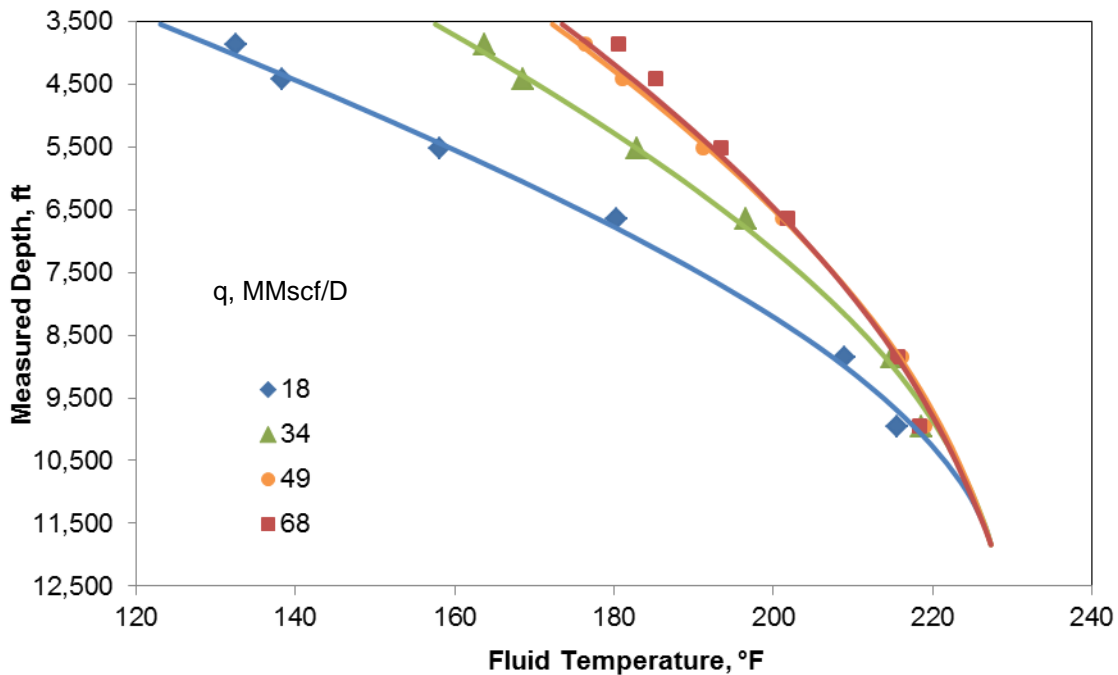


Figure 6 – History matching temperature profiles at various rates for Well 3.

As expected the match starts to suffer at higher rates. This is due to the phenomenon called Joule-Thompson cooling. This point was also made recently by Kabir et al. (2014). Similar to Figure 5, **Figure 7** shows the history matching of temperature profiles at various depths. Here we show results from more gauges. There are quite a few gauges towards the bottom which may appear redundant but are usually placed as backups due to high rate of gauge failure at the bottomhole.

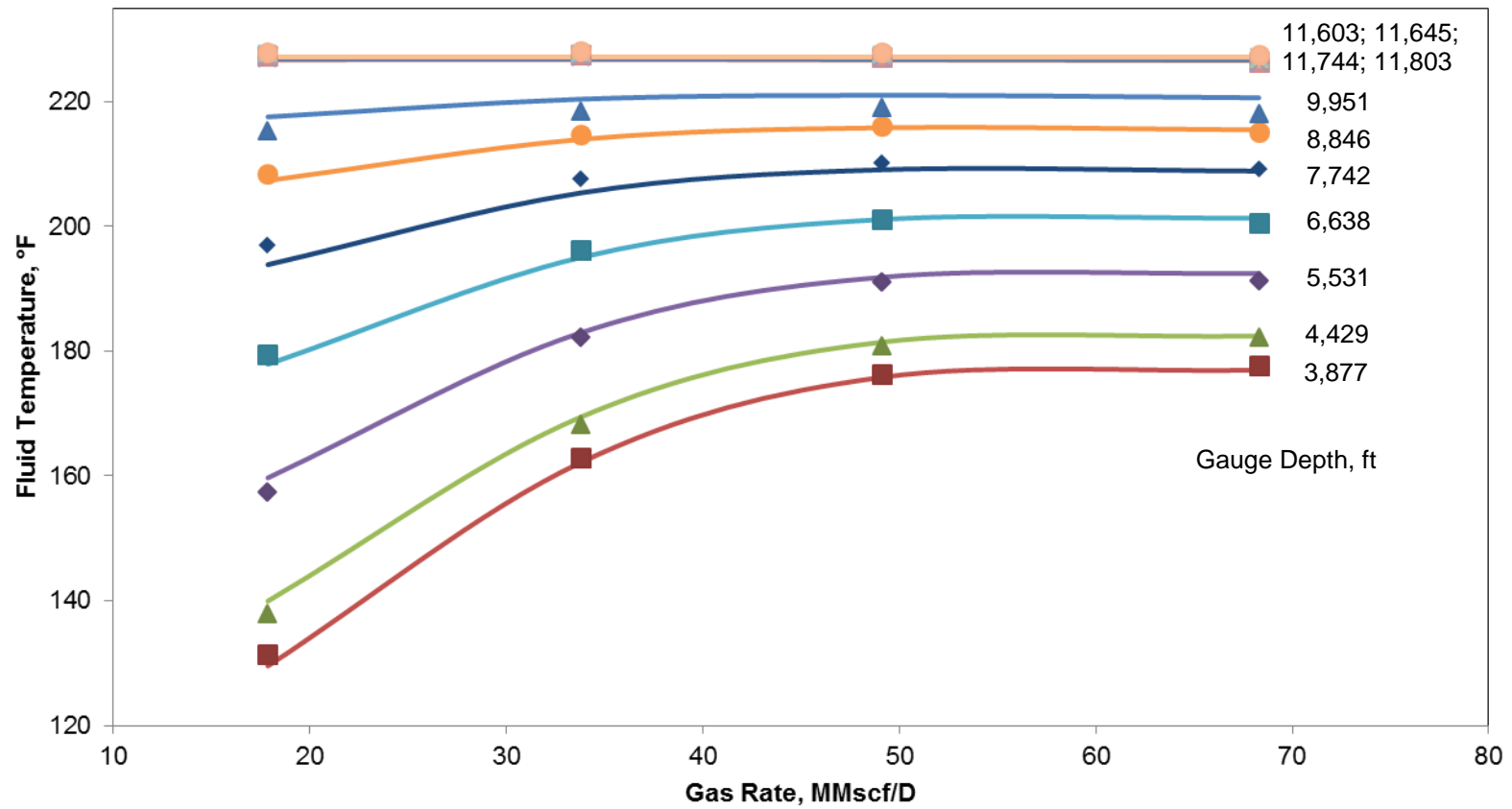


Figure 7 – History matching temperature profiles at various depths for Well 3.

All the gauges shown in Figure 7 are neither needed nor were used for the estimation. Using multiple gauges, after a certain number of gauges the model reaches a diminishing rate of return. Use of more gauges after that does not add much utility to the inversion process. Moreover the data near the bottomhole lacks the fidelity as well that the model relies on to estimate rates.

Table 4 presents the error analysis for the rate estimation process.

	Flow Rate, MMscf/D			
	Rate 1	Rate 2	Rate 3	Rate 4
Computed	16.49	33.98	56.10	76.26
Measured	17.89	33.80	49.10	68.30
Error (%)	-7.85	0.54	14.26	11.65

Table 4 – Error estimation in computed rates, Well 3.

The rather large error for the last two rates is related to the Joule-Thompson cooling effect as described earlier.

Transient Modeling

Similar analysis was carried out for the two wells already mentioned using the transient model developed in the previous chapter. Additionally, another well was studied under the same premise. This well, Well 4 provided a unique opportunity to illustrate the strength of transient modeling. In this section, we show all three wells and the forward modeling results. However we focus mainly on Well 4 for this section of the analysis.

For all three wells transient fluid temperature data over more than 100 hours were available for multiple flow rates at various well depths. **Figure 8** shows data from five of those stations for Well 4.

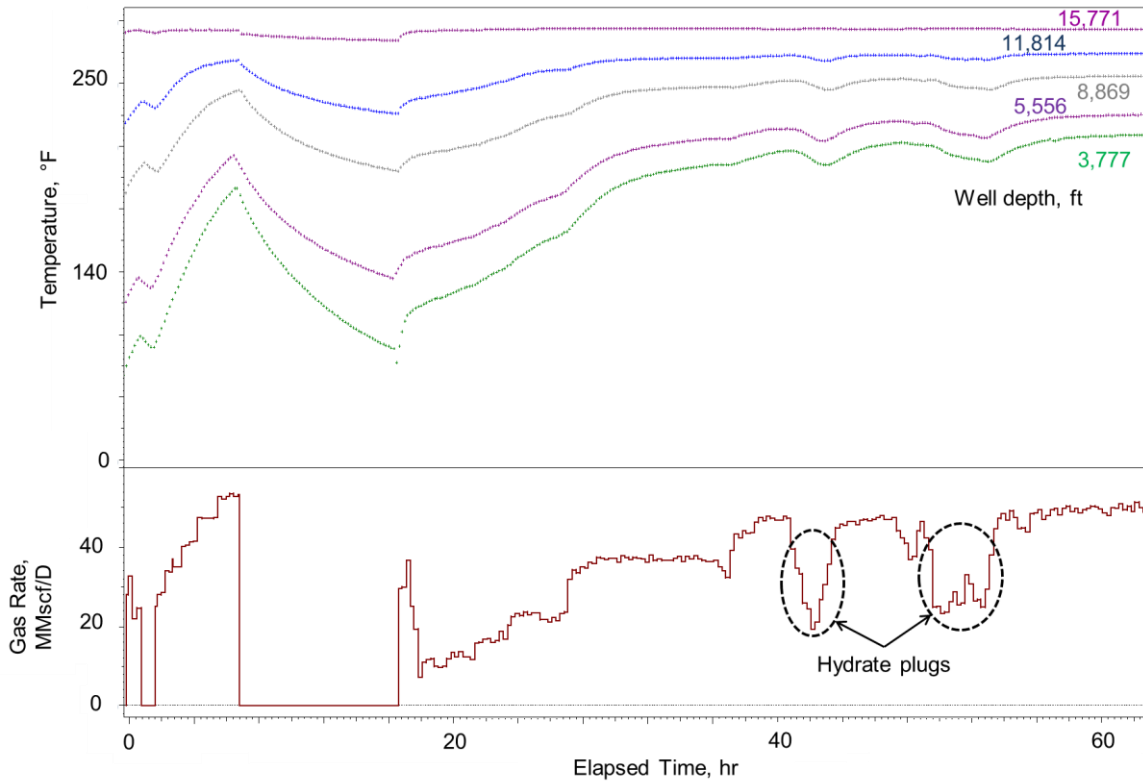


Figure 8 – Depth-dependent measurements of transient temperature in Well 4.

Figure 8 illustrates a number of interesting phenomena that characterize the transient fluid-temperature behavior. One such characteristic evident is the distinctly varying temperature profiles near the mudline while a near-flat line represents the profile close to the bottomhole. The explanation of this gradual flattening of the temperature profiles with increasing depth is simple. Fluid entering the wellbore is at (or nearly at) the same

temperature as the formation. Therefore, near the bottomhole, there is little or no difference between the fluid temperature T_f and the surrounding formation T_{ei} . Because $T_f - T_{ei}$ is the driving force for heat transfer, not much heat exchange occurs near the well bottom, which explains the relatively unperturbed temperature profile with time at deeper stations. In contrast, near the mudline the formation surrounding the fluid is at a much lower temperature than the fluid itself. This larger temperature contrast at shallower depths explains the greater heat exchange.

For the same amount of heat exchange, however, temperature change is smaller for greater rates (because $Q \sim mc_p \Delta T$). Therefore, at higher flow rates the fluid temperature will stay higher than for a lower rate because of a smaller temperature difference. This behavior is observed in the temperature profiles at 2 to 6 hours. During this period, rates keep increasing, resulting in increasing fluid temperature with rate and, therefore, with time.

When fluid flow is initiated from a shut-in well (or when a step increase in rate occurs), the fluid temperature increases for some time, even if the rate is kept constant. This point is illustrated in **Figure 9**, wherein at each constant-rate segment, the fluid temperature increases by about 15°F. This phenomenon is easier to understand for a rate increase than for a rate decrease; although, the same explanation applies to both situations. When a rate increase is initiated and held constant for some time, hotter fluid from greater depth moves up and replaces the colder fluid at any given position. As production

continues, increasingly hotter fluid from greater depths does the replacement, thereby allowing the fluid temperature to increase with time at any elevation higher than the point of fluid entry. However, after the bottomhole fluid has replaced the fluid at a given location, the temperature change reaches a point of diminishing returns for a given rate. In other words, this location reaches a pseudosteady-state temperature for a given rate.

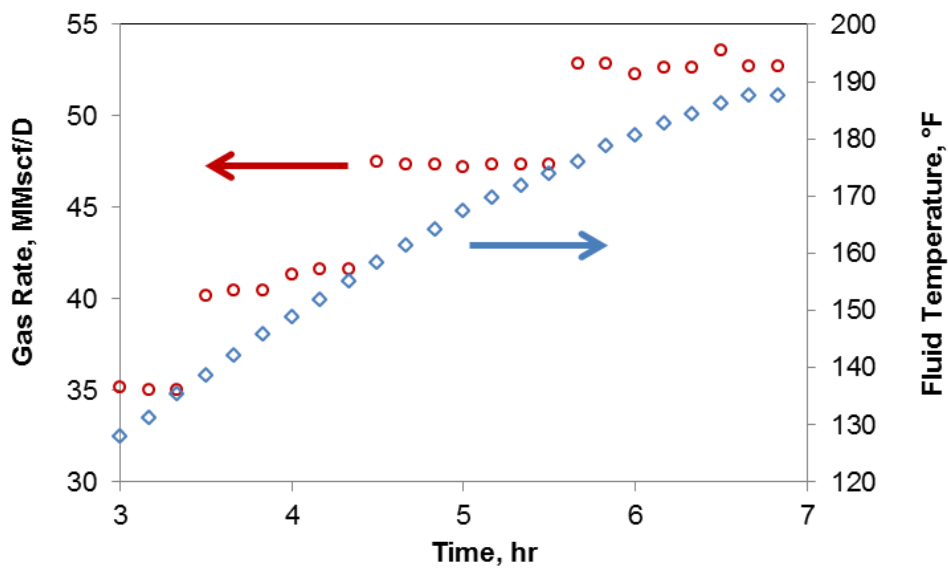


Figure 9 – Gas Rate and Fluid Temperature during the cleaning phase in Well 4.

Below we offer both verification and validation of the transient temperature model. In addition to the data from the three wells mentioned above, we also used temperature estimation from a commercial software package (WELLCAT) to verify our model. The finite-element wellbore simulator uses a detailed description of the wellbore, fluid, and formation to generate transient solution for the flow problem at hand. The simulator estimates temperature profile based on the rate history where temperature at the end of a

rate step is used as an initial condition for the next rate step. Although this simulator is intended for casing design, it solves the heat flow problem of interest in a rigorous fashion. However the simulator is not capable of inverse modeling. Therefore it was only used to validate forward model.

Well 2

The details of the input parameters used for Well 2 are presented in Table 1. Bottomhole pressures known at each time step are tabulated in Appendix A. **Figure 10** presents the history matching effort of the temperature profile near the mudline for the well. The good agreement of the model with data provides validation and the commercial simulator verifies the results. As noted earlier, only one set of input parameters was used for history matching temperature data from all depths and rates for all three wells in this study.

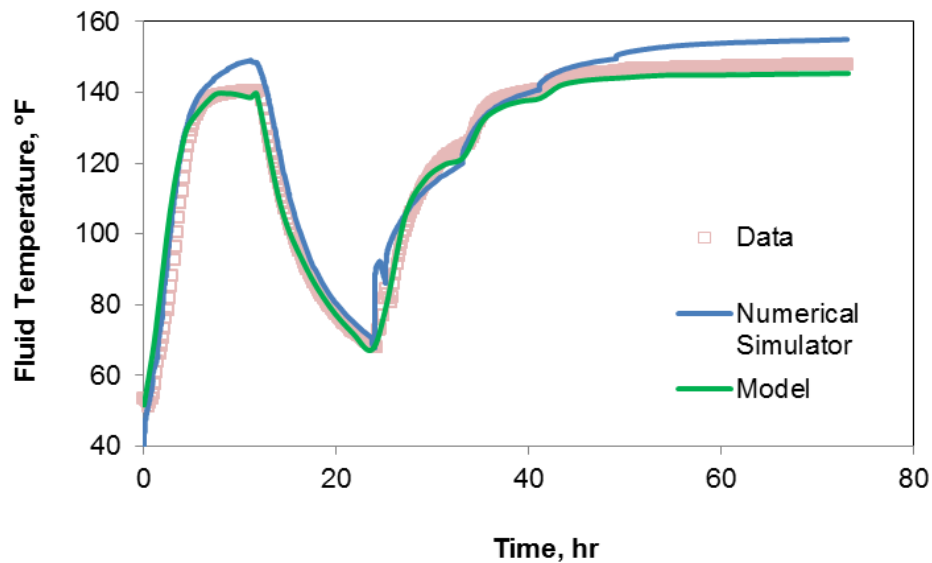


Figure 10 – History matching transient temperature profile, Well 2.

As shown in Figure 10, Well 2 depicts a classical temperature profile for a flow-after-flow test, following the cleanup and shut-in periods. The initial period from well startup until about 12 hours corresponds to the cleanup phase wherein the rate is continually increased in a stepwise fashion. After this period of activity, the well is shut in for about the same period. Following the shut-in, the flow-after-flow test for deliverability, in which the surface rate is increased in each successive step for the same duration, is initiated. This succession of rate profile is accurately captured by the temperature profile. At the start of the test (at approximately 25 hours), the temperature increases due to the hotter fluid rising up the wellbore. The temperature starts to stabilize at around 33 hours when another increase in rate causes the temperature to rise farther. Although the time is the same, this increase in temperature is not the same as with the previous rate.

This reduced response is triggered by the decreasing temperature difference between the fluid and the wellbore as mentioned earlier.

Well 3

As in the case of steady-state modeling, analysis similar to Well 2 was applied to Well 3 as well. Input parameters for Well 3 are presented in Table 3. Bottomhole pressures known at each time step are tabulated in Appendix A. Verification with a commercial simulator and data validation is shown in **Figure 11**.

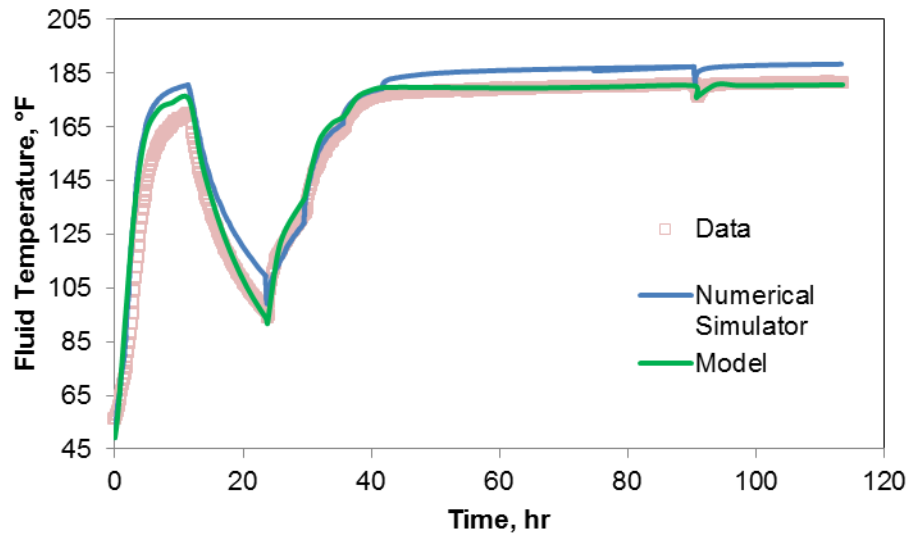


Figure 11 – History matching transient temperature profile, Well 3.

The profiles reasonably match the data. One interesting thing to note over here is the dip in the temperature profile around 90 hours. This dip is a manifestation of a sudden drop

in flow rate around the same time as shown in Figure 3. Such sensitivity bodes well during the inverse modeling to predict rate.

Well 4

The same reasoning applies to Well 4 which follows a similar rate schedule. Input parameters for Well 4 are presented in **Table 5** and bottomhole pressures in Appendix A. During the production from Well 4, hydrates were formed in the wellbore. As Figure 8 shows, this plugging occurred around 42 and 52 hours. The problem was mitigated by methanol injection. However, the benefit of using temperature measurements to estimate flow rate becomes more evident here because this anomaly is captured by the fluid temperature and successfully reproduced by the model and the commercial simulator, as **Figure 12** and **Figure 13** demonstrate.

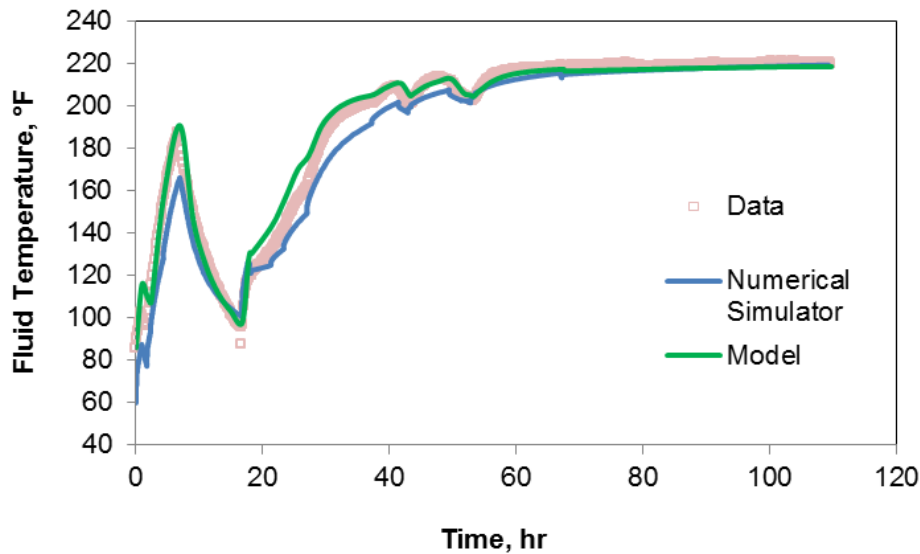


Figure 12 – History matching transient temperatures profile, Well 4.

Total Vertical Depth, ft	15,347
Measured Depth, ft	16,434
Inclination	24
Pipe Roughness, ft	0.00001
Tubing ID, in.	3 4/5
Tubing OD, in.	4.5
Casing ID, in.	8 15/22
Casing OD, in.	9 5/8
Cement ID, in.	9 5/8
Cement OD, in.	13
Mudline Temperature, °F	86
Bottomhole Temperature, °F	273
Coefficient of Thermal Expansion (β), 1/°F	0.00011
Critical Pressure, psia	671.14
Critical Temperature, °R	367.74
Specific gravity of gas	0.643
Thermal conductivity of tubing fluid, Btu/(hr-ft-°F)	0.03
Thermal conductivity of tubing and casing, Btu/(hr-ft-°F)	26
Thermal conductivity of annulus fluid, Btu/(hr-ft-°F)	0.3
Thermal conductivity of cement, Btu/(hr-ft-°F)	0.6
Thermal conductivity of formation, Btu/(hr-ft-°F)	1
Specific heat of gas, Btu/(lbm-°F)	0.78
Specific heat of annular fluid, Btu/(lbm-°F)	1
Density of annular fluid, lbm/ft ³	67.15
Viscosity of annular fluid, cp	0.6
Geothermal gradient, °F/ft	0.01615

Table 5 – Input parameters for Well 4.

Figure 13 shows the history match of transient temperature profiles done at various depths. For clarity of presentation, only three depths are shown, but in reality, we have had 10 depths (each 1,000 ft apart) to anchor the model solution. As expected, the

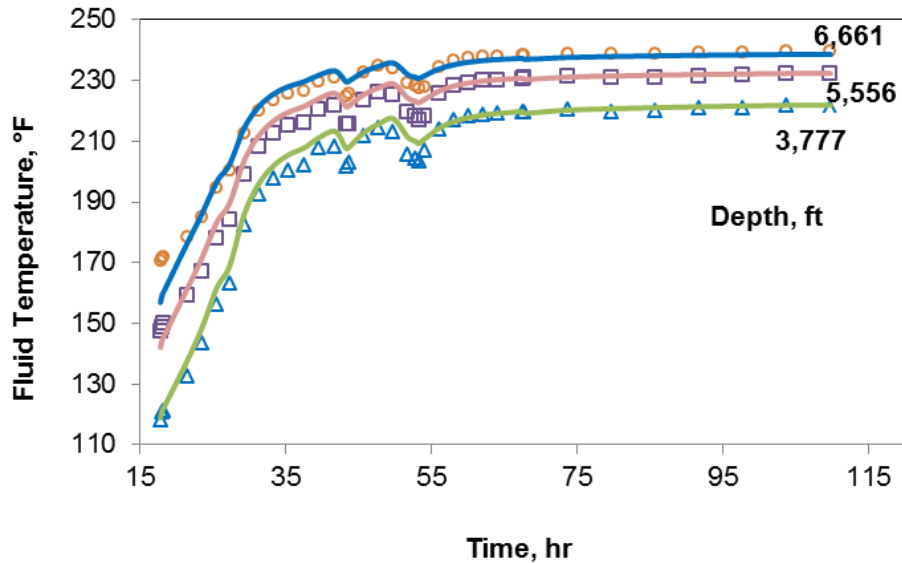


Figure 13 – History matching transient temperature profiles using data at different depths, Well 4.

fidelity of the temperature response decreases with increasing depth. Yet, the decrease in flow rate is captured at greater depths as well. Such spatial data help in accurate estimation of the fluid flow rates because multiple datasets constrain the problem at hand. This point is illustrated more clearly in **Figure 14**, which shows the rate history match based on the temperature matches in Figure 13.

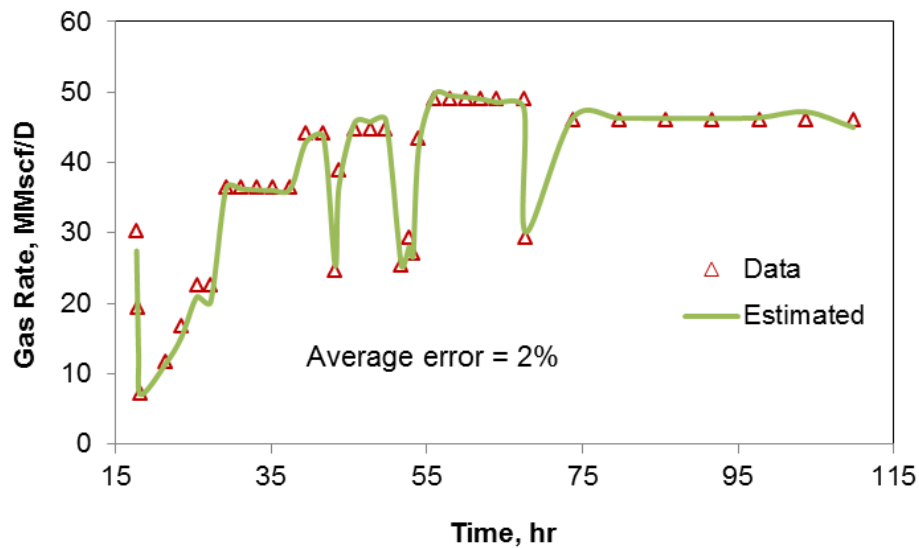


Figure 14 – Estimated rate profile using temperature data at different depths, Well 4.

As shown in Figure 14, the predicted rates closely follow those recorded using the multiphase flow meter. The model’s sensitivity enables it to capture the flow rate restrictions around 42 and 52 hours.

A problem that often creeps up during inverse modeling is the solution non-uniqueness. This aspect is often the case in inverse problems because the problem is often under defined. However, temperature data at multiple depths make up for the lack of under defined parameters. That said, we cannot ignore that more often than not such rich data are lacking in most test settings. Usually the temperature data is limited to the wellhead and bottomhole conditions. Therefore, we employed the same methodology discussed earlier on temperature data from just one depth nearest to the mudline, which is

construed as most appropriate for the analysis because of the largest temperature response.

Figure 15 offers the results for the history matching of temperature estimates and **Figure 16** presents the rate estimated based on the match shown in Figure 15. As shown, the match quality for the temperature is not much different; however, the rate quality suffers slightly. Here, the non-uniqueness of the inverse problem becomes more evident during our analysis because the problem becomes less constrained. This experience suggests that the model be calibrated and anchored for a known rate to achieve more confidence in the prediction when using data from a single location.

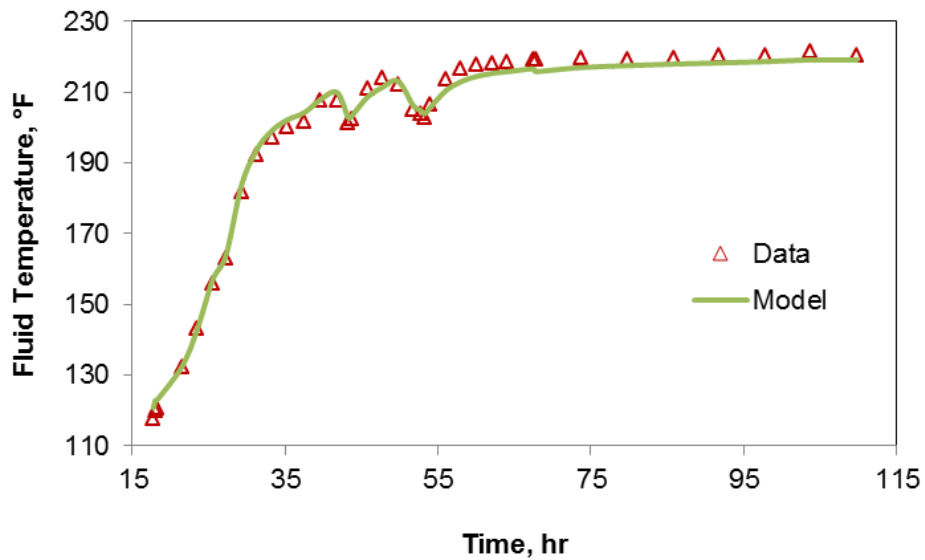


Figure 15 – History matching transient temperature profile using data nearest to the mudline, Well 4.

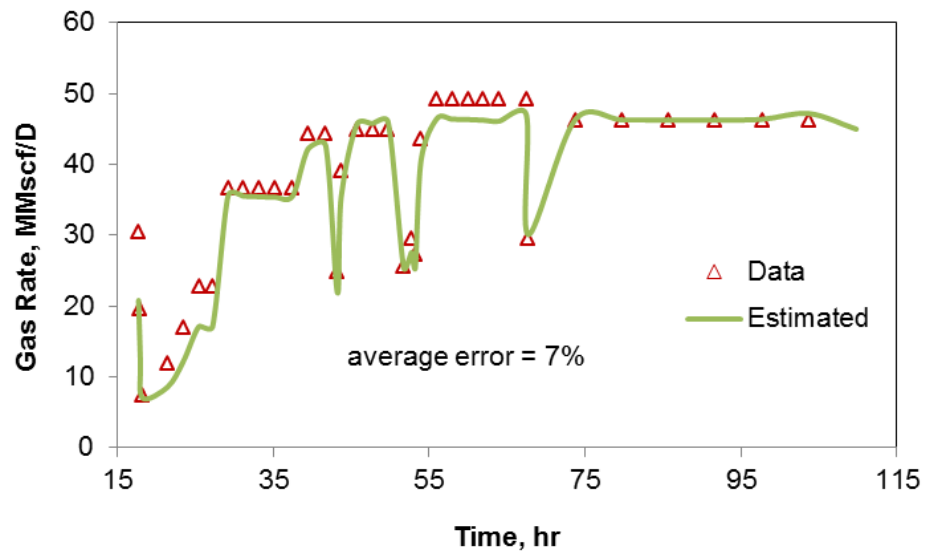


Figure 16 – Estimated rate profile using temperature data nearest to the mudline, Well 4.

Summary

Application of the models developed in the previous chapter is shown for both steady-state and transient temperature models. Three different wells are discussed in this chapter for the purpose of model verification and validation. Inverse modeling is demonstrated for all three wells as well. Though the availability of data at different depths provide for more faith in the modeling and inversion, rate can be estimated using just one depth. In such case, it is suggested to calibrate the model against known rates before applying the algorithm to a rate estimation exercise.

CHAPTER V

FIELD APPLICATION

Introduction

So far we discussed how fluid temperature in the wellbore can be estimated with time at any depth. The technique facilitates inverse modeling and the estimation of rate as it changes with time in the wellbore. This chapter highlights how this method can be made use of on the field to obtain useful and much needed information.

In most settings, the cleanup period is overlooked from a transient-test interpretation standpoint. This is primarily because rates are seldom metered with a multiphase flow meter. Obviously, continuously changing the two-phase flow situation presents additional challenges in test interpretation. However, if rates of the dominant phase are inferred from distributed temperature measurements, reliable estimations of relevant reservoir parameters may be obtained. These estimated parameters, in turn, can be used to fine-tune the subsequent test sequence, thereby saving considerable expense.

This chapter demonstrates the applicability of the proposed rate-estimation model from the distributed-temperature data by verifying its performance with a field example, Well 4. We also validate the usefulness of cleanup data analysis with a simulated example. The simulated example was generated with a commercial numerical model, wherein

fluid invasion was mimicked by injecting water into the formation and producing gas thereafter by imposing step-wise increase in drawdown at sandface. The use of statistical design of experiments (DOE) provides clues about the relative importance of input parameters.

Estimating Reliable Rates with Temperature Modeling

Rates are estimated through an overall temperature match at various depths by honoring discrete temperature data at the end of each time period. **Figure 17** depicts the temperature data and estimates using the rigorous transient model (Eq. 31) for the early cleanup phase of Well 4. An important observation in Figure 17 is the smooth nature of the temperature profile, which may lead one to think that the rise in temperature was because of production period alone. That, however, is not the case. In fact, the cleanup fluid flow rate changed significantly and irregularly over time.

Figure 18 provides a comparison between the estimated rates using the described methodology and the measured rates during the early cleanup phase in Well 4. As Figure 18 points out, the transient temperature modeling allows for the determination of rate. Despite the steady increase of temperature, Figure 18 satisfactorily captures the fluctuations in rate. The ability to obtain such information can have great impact on transient testing. With the pressure measurements already available using downhole telemetry, the requirements for transient testing is satisfied with this information. This is discussed more in the next section.

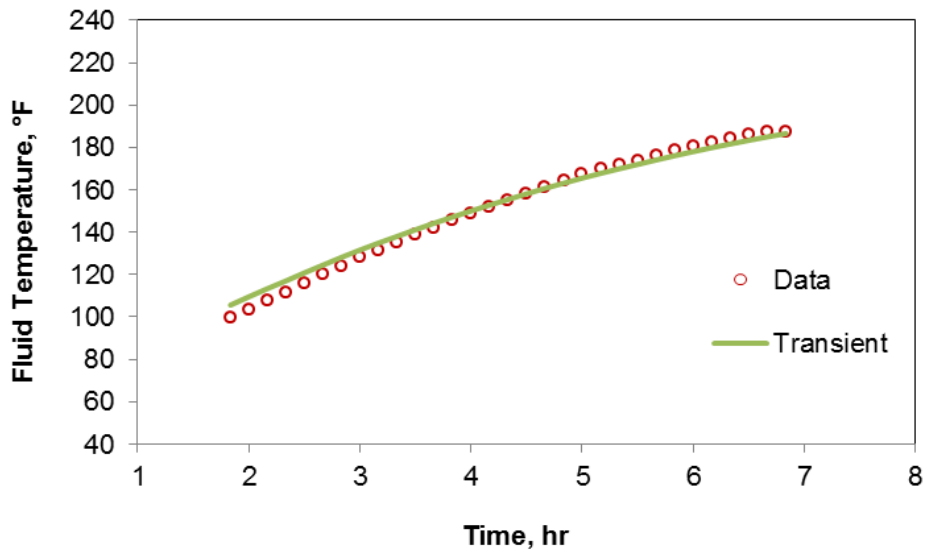


Figure 17 – Temperature history matching using transient and steady-state models for cleanup phase, Well 4.

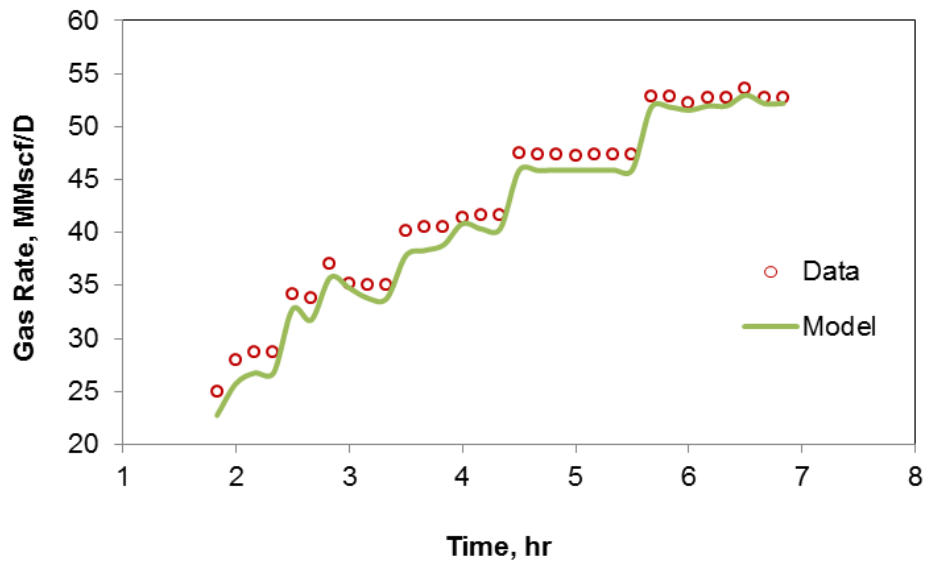


Figure 18 – Comparison of measured and estimated rates during the cleanup phase, Well 4.

It was speculated that the effect of superposition is not significant in this analysis. To investigate this, simulations with and without superposition were carried out. **Figure 19** shows the differences in the temperature estimated with and without superposition for one of the rate schedules during the cleanup phase. As the figure shows, the superposition in heat flow does not play a significant part for this flow problem at hand.

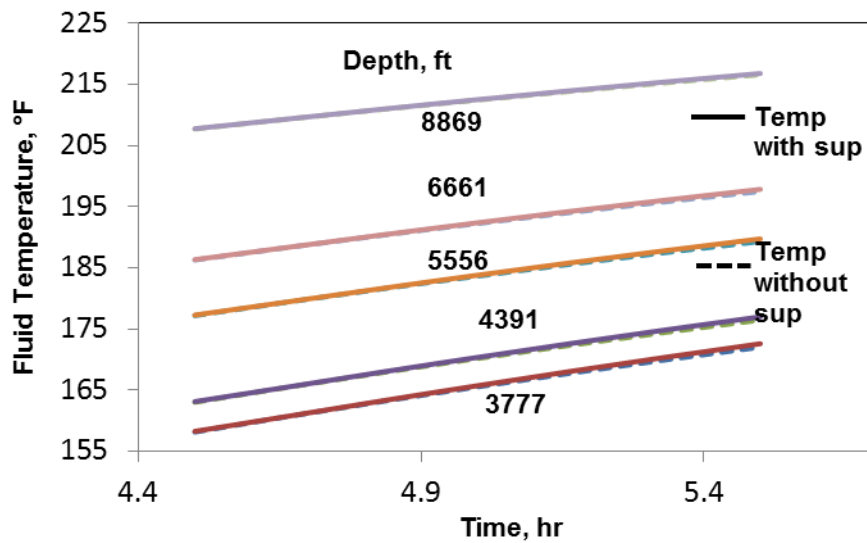


Figure 19 – Temperature estimation at different depths with and without superposition for cleanup phase, Well 4.

However, some important items worthy of note confirm the notion of decreasing heat transfer rate with time. As time progresses, the fluid temperature estimated with superposition tends to be slightly higher than without superposition. This observation confirms that the difference in temperature between the wellbore fluid and the formation is decreasing due to the formation being heated up, thereby decreasing the heat transfer rate as highlighted above. Therefore, the fluid temperature with superposition is slightly

higher. Another observation is that the effect of superposition declines with increasing depth. This outcome makes intuitive sense in that the difference between the formation and the fluid temperature declines with increasing depth.

Cleanup Effect in Pressure-Transient Response

In this section, we use both synthetic and field examples to explore the effect of cleanup in our ability to obtain reservoir permeability. The underlying thought is to obtain a good estimation of permeability so that the post-cleanup flow and shut-in periods can be fine-tuned. We resort to the statistical DOE to do an objective analysis. To that end, we generate solutions with a numerical simulator by injecting water into the formation to mimic fluid invasion, followed by a rest period and a sequence of flow and shut-in periods, as depicted in the rate profile in **Figure 20** and **Figure 21**. Figure 20 shows the two buildups: one after the cleanup and the second after the flow-after-flow test. The parameters obtained from the two buildup analyses confirm the hypothesis that the same permeability estimate can be obtained from the two tests. We compared the results of two buildups from one of the worst cases considered in this study in terms of depth of invasion. The underlying idea was to underscore the point that permeability is well estimated during or following the incomplete cleanup period. As **Figure 22** suggests only the skin is impacted, not the formation kh . Let us study the results of the DOE to learn more about the effect of skin.

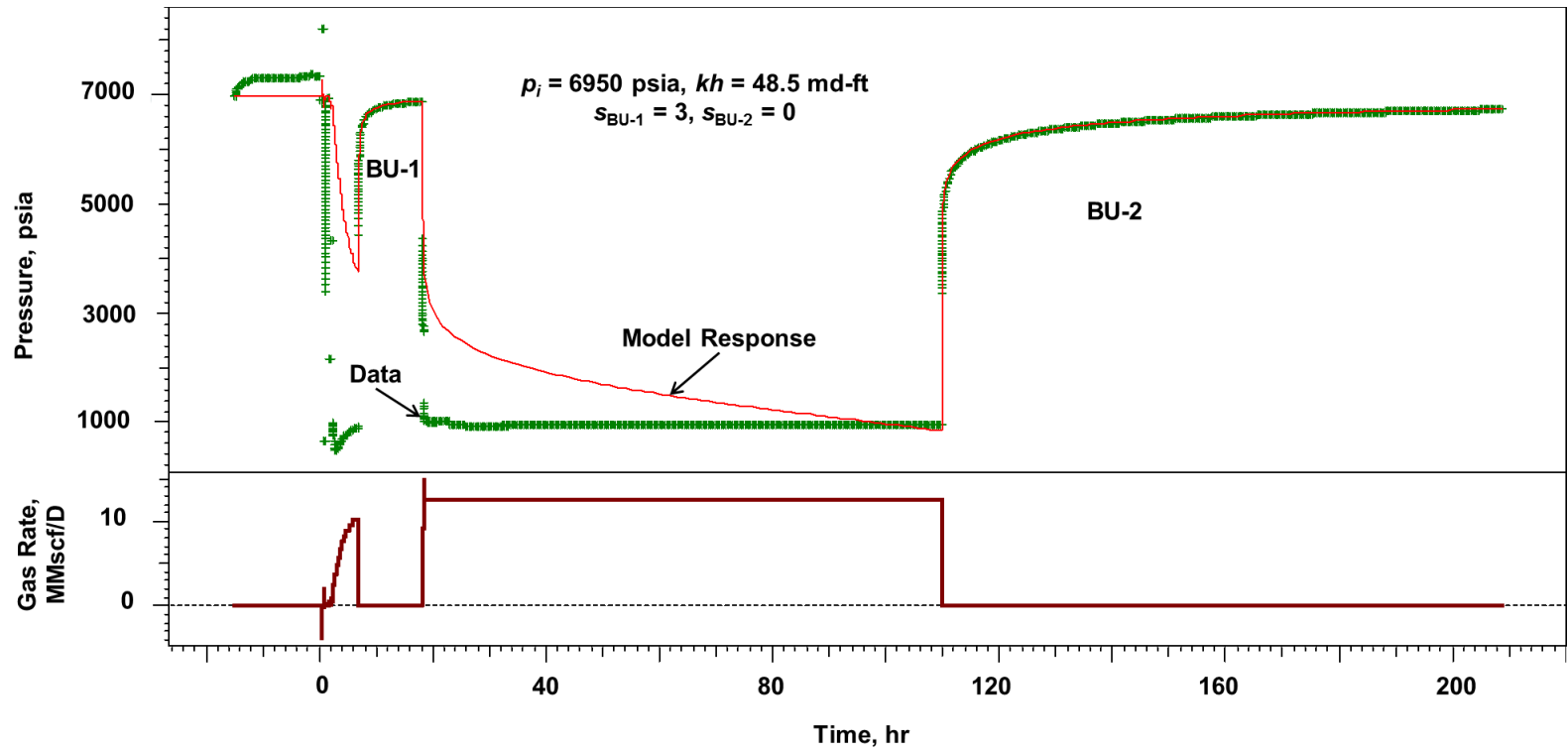


Figure 20 – Pressure simulation for one of the design cases.

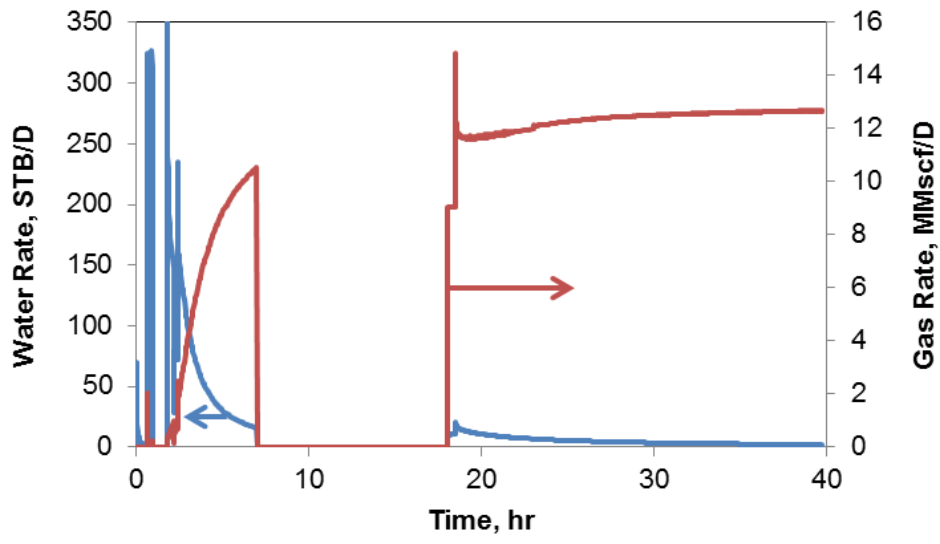


Figure 21 – Rate simulation for the same case as Fig. 20.

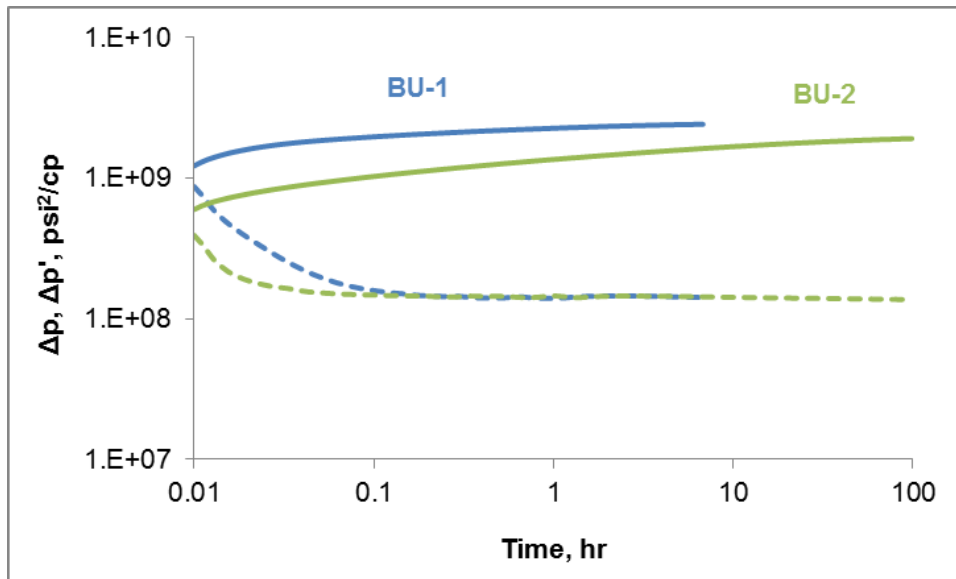


Figure 22 – Buildup charts for the same case as in Fig. 10.

Table 6 presents the design variables for the full-factorial analysis. The summary of these flow-simulation runs are presented in **Figure 23** and **Figure 24** on Pareto charts. In this DOE, skin for both the shut-in periods is the dependent variable, whereas formation conductivity, depth of mud-filtrate invasion, and the initial shut-in time before production constituted the three independent variables. As noted in some of the skin values associated with the second buildup, formation cleanup is not guaranteed in adverse situations when deep filtrate invasion occurs, coupled with inadequate flow periods and/or insufficient drawdown. This point is made clearly in Figure 21 wherein the water continues to be produced long after the cleanup, thereby affecting the skin for the second buildup.

	<i>kh</i> , md-ft	depth of invasion, ft	Initial shut-in time, hr
Low	50	1	0
Medium	1500	2	10
High	4000	3	24

Table 6 – Design variables for full factorial analysis.

The positive sign associated with any independent variable on the Pareto chart suggests that an increase of the independent variable will result in an increase of the dependent variable. Although *kh* is by far the dominant variable, the Pareto chart does not imply that the other two variables with absolute t-test value below 95% confidence level are

not influencing the skin in the second buildup test. Rather, the chart shows that they are statistically insignificant within the 95% confidence interval.

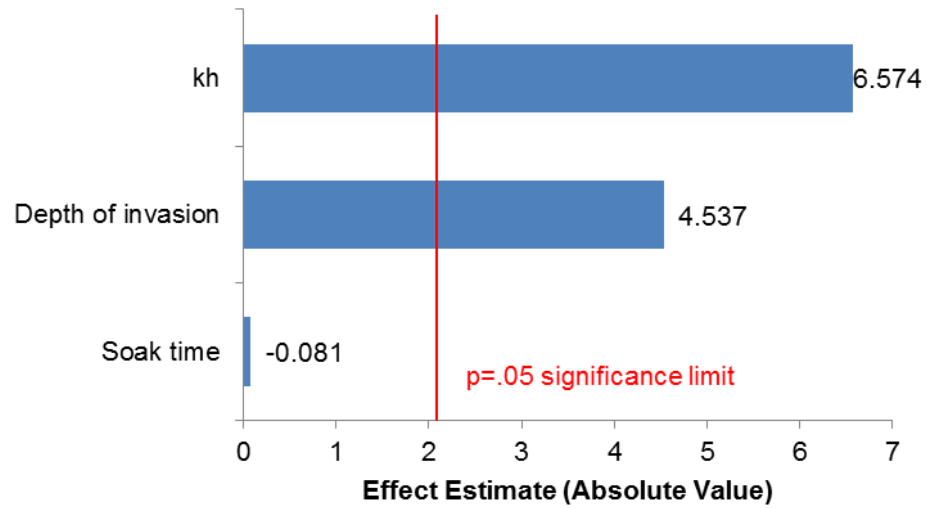


Figure 23 – Pareto chart showing the significance of independent variables in skin from BU-1.

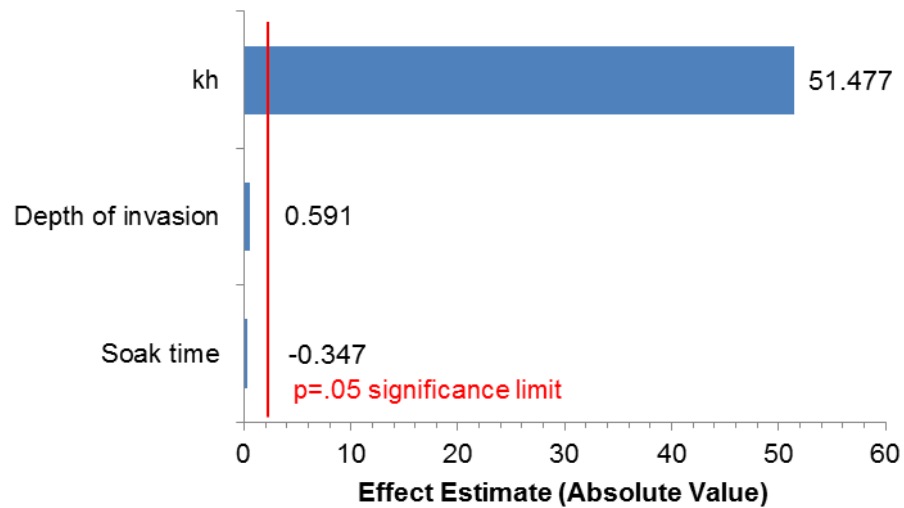


Figure 24 – Pareto chart showing the significance of independent variables in skin from BU-2.

As the results of the DOE with the simulated example show, the skin is dominated by the formation's conductivity or the kh product. Interestingly, the other significant variable for the pre-cleanup skin is the depth of invasion. However, the significance of filtrate invasion diminishes in the second buildup, reaffirming the contention that the difference in the pre- and post-cleanup response manifests in terms of skin. This point is made by **Figure 25**, which shows the results of pre- (BU-1) and post-cleanup (BU-2) shut-in periods. As expected, the derivative signatures overlay suggests the same conductivity, but the pressure-difference curves separate indicating the skin effect or incomplete cleanup.

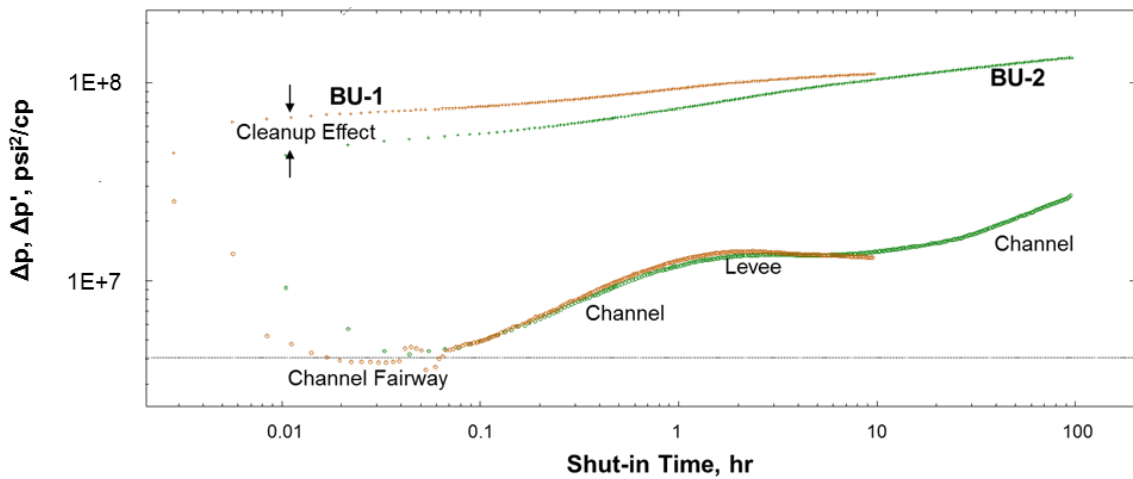


Figure 25 – Incomplete cleanup manifests in terms of skin, Well 4.

The analysis in the last few pages strongly suggests that the same permeability can be gauged from the pre-cleanup transient response as from the post-cleanup. The only issue which remains then is the availability of reliable rates for the pre-cleanup period. The

example shown in this and the previous section, therefore, is a demonstration of how those rates can be obtained from measurements that are already made in most DST settings.

Summary

This chapter presents how the models and the methodology presented till the last chapter can be made use of in a unique way to help with drill-stem testing. Rates are estimated, using the same analysis as presented, for the cleanup period in Well 4. Those rates are then shown to convey reliable permeability estimates through analysis of transient testing techniques. It is shown that the difference seen in the buildup derivatives response is due to skin and not permeability which provides assurance that the flow-after-flow test can be designed/fine-tuned according to the already estimated parameters. Thus, considerable expense can be saved in term of rig time costs and avoiding test design failures.

CHAPTER VI

DISCUSSION AND CONCLUSION

This thesis presents steady-state and transient temperature models for predicting flowing fluid temperature in the wellbore. The models presented are based on the work of Hasan and Kabir (1994) and Hasan et al. (2005). A novel depth-dependent temperature superposition approach was used to arrive at the analytical formulations. The superposition principle accounts for the variable heat flux between the wellbore fluid and the formation which was held constant in all the models in literature prior to this work. The study also demonstrates the use of temperature measurements made at several depths in estimating flow rates in dry-gas wells. The multiphase flow meter and surface separator verified these rates for all three wells. A commercial, numerical wellbore simulator lends further credence to the analytical solution presented here for the transient model. Although the solution becomes robust when multiple discrete temperature data sets become available at various depths, the use of single data set at the wellhead is also feasible for estimating rates as outlined here. Successful implementation of rate estimation, within engineering accuracy, is shown for both steady-state and transient cases.

This study accounts for the effect of formation heating in the form of a variable ξ to account for the depth-dependent superposition effect. However, ξ did not turn out to be

greatly significant for the field flow problem studied. Nonetheless, we surmise that this parameter will play a more significant role in different circumstances. To begin with, the importance of ζ can be gauged by comparing it with the value of ψ in the model. If ζ is insignificant compared to the value of ψ , it might not cause a significant effect. Conversely, if ζ is significant in comparison to ψ , ignoring it may lead to inaccuracy of the estimated rates. This situation may arise in cases where the resistance between the wellbore and the formation is higher than usual, such as in presence of vacuum-insulated tubing. Another example of reduced heat loss arises at late times when the formation has had a chance to heat up after a considerable production period.

Interpretation of transient-pressure data for both pre- and post-cleanup periods suggested that formation permeability is unaffected by the two-phase flow effects. Stated differently, only the skin is different in the two analyses. The use of statistical DOE provided the initial clue. For instance, a combination of independent variables, such as the permeability-thickness product, soak period, and radius of mud-filtrate invasion collectively suggested that permeability was reproduced without any error. The convergence of the derivative plateaus supports this notion, but the difference in the corresponding pressure curves is a reflection of skin. Both synthetic and field examples lend credence to this point. Estimating the formation permeability up front allows fine-tuning of the subsequent test periods commensurate with objectives.

Though the models seem to work really well, we would still like to make some suggestions for any further improvement or incremental work done on the same subject. Some of the assumptions that were made in this study could be avoided and the modeling looked at in a more robust manner. The models presented assume some of the thermal properties to be constant, e.g. specific heat capacities and thermal conductivities are assumed to stay constant throughout the wellbore. The thermal storage parameter, C_T , is also assumed to be a constant value as mentioned before. Though the model has the ability to handle changes in the wellbore diameter, it was largely kept constant for the purpose of modeling. Moreover, the variation of the superposition variable, ξ , with well depth was ignored in the initial derivation of the model. However it was accounted numerically in the numerical implementation. Most of these assumptions would not incur significant effects on the temperature models. However, for the purpose of more accurate modeling and making the model more sound theoretically, some of these assumptions can be removed in future works.

REFERENCES

- Alpak, F. O., H. Elshahawi, M. N. Hashem et al. 2008. Compositional Modeling of Oil-Based-Mud-Filtrate Cleanup During Wireline Formation Tester Sampling. *SPE Reservoir Evaluation & Engineering* **11** (2): 219-232.
<http://dx.doi.org/10.2118/100393-PA>.
- Alves, I. N., F. J. S. Alhanati, O. Shoham. 1992. A Unified Model for Predicting Flowing Temperature Distribution. in Wellbores and Pipelines. *SPE Production Engineering* **7** (4): 363-367. <http://dx.doi.org/10.2118/20632-pa>.
- Bahonar, M., J. Azaiez, Z. J. Chen. 2011a. Transient Nonisothermal Fully Coupled Wellbore/Reservoir Model for Gas-Well Testing, Part 1: Modelling. *Journal of Canadian Petroleum Technology* **50** (9-10): 37-50.
<http://dx.doi.org/10.2118/149617-pa>.
- Bahonar, M., J. Azaiez, Z. J. Chen. 2011b. Transient Nonisothermal Fully Coupled Wellbore/Reservoir Model for Gas-Well Testing, Part 2: Applications. *Journal of Canadian Petroleum Technology* **50** (9-10): 51-70.
<http://dx.doi.org/10.2118/149618-pa>.
- Clarkson, C. R., H. Behmanesh, L. Chorney. 2013. Production-Data and Pressure-Transient Analysis of Horseshoe Canyon Coalbed-Methane Wells, Part II: Accounting for Dynamic Skin. *Journal of Canadian Petroleum Technology* **52** (1): 41-53. <http://dx.doi.org/10.2118/148994-pa>.

- Curtis, M. R., E. J. Witterholt. 1973. Use of the Temperature Log for Determining Flow Rates in Producing Wells. *Las Vegas, Nevada: Society of Petroleum Engineers.*
<http://dx.doi.org/10.2118/4637-MS>.
- Duru, O. O., R. N. Horne. 2010. Joint Inversion of Temperature and Pressure Measurements for Estimation of Permeability and Porosity Fields. *Florence, Italy: Society of Petroleum Engineers.* <http://dx.doi.org/10.2118/134290-MS>.
- Edwardson, M. J., H. M. Girner, H. R. Parkison et al. 1962. Calculation of Formation Temperature Disturbances Caused by Mud Circulation. *Journal of Petroleum Technology* **14** (4): 416-426. <http://dx.doi.org/10.2118/124-PA>.
- Fan, L., W. J. Lee, J. P. Spivey. 2000. Semi-Analytical Model for Thermal Effect on Gas Well Pressure-Buildup Tests. *SPE Reservoir Evaluation & Engineering* **3** (6): 480-491. <http://dx.doi.org/10.2118/68020-pa>.
- Gao, G., Y. Jalali. 2008. Prediction of Temperature Propagation Along a Horizontal Well During Injection Period. *SPE Reservoir Evaluation & Engineering* **11** (1): 131-140. <http://dx.doi.org/10.2118/96260-pa>.
- Glasbergen, G., D. Gualtieri, M. S. V. Domelen et al. 2009. Real-Time Fluid Distribution Determination in Matrix Treatments Using DTS. *SPE Production & Operations* **24** (1): 135-146. <http://dx.doi.org/10.2118/107775-pa>.
- Glasbergen, G., V. J. Yeager, R. P. Reyes et al. 2010. Fluid-Diversion Monitoring: The Key to Treatment Optimization. *SPE Production & Operations* **25** (3): 262-274. <http://dx.doi.org/10.2118/122353-pa>.

- Goode, P. A., R. K. M. Thambynayagam. 1996. Influence of an Invaded Zone on a Multiprobe Formation Tester. *SPE Formation Evaluation* **11** (1): 31-40.
<http://dx.doi.org/10.2118/23030-pa>.
- Guo, B., S. Duan, A. Ghalambor. 2006. A Simple Model for Predicting Heat Loss and Temperature Profiles in Insulated Pipelines. *SPE Production & Operations* **21** (01): 107-113. <http://dx.doi.org/10.2118/86983-PA>.
- Hagoort, J. 2004. Ramey's Wellbore Heat Transmission Revisited. *SPE Journal* **9** (04): 465-474. <http://dx.doi.org/10.2118/87305-PA>.
- Hagoort, J. 2005. Prediction of Wellbore Temperatures in Gas Production Wells. *Journal of Petroleum Science and Engineering* **49** (1): 22-36.
<http://dx.doi.org/10.1016/j.petrol.2005.07.003>.
- Hasan, A. R., C S. Kabir, C. Sarica. 2002. *Fluid Flow and Heat Transfer in Wellbores*, Society of Petroleum Engineers Richardson, TX (Reprint).
- Hasan, A. R., C. S. Kabir, X. Wang. 2009. A Robust Steady-State Model for Flowing-Fluid Temperature in Complex Wells. *SPE Production & Operations* **24** (02): 269-276. <http://dx.doi.org/10.2118/84288-PA>.
- Hasan, A. R., C. S. Kabir. 1994. Aspects of Wellbore Heat Transfer During Two-Phase Flow. *SPE Production & Facilities* **9** (3): 211-216.
<http://dx.doi.org/10.2118/22948-pa>.
- Hasan, A. R., C. S. Kabir, D. Lin. 2005. Analytic Wellbore Temperature Model for Transient Gas-Well Testing. *SPE Reservoir Evaluation & Engineering* **8** (3): 240-247. <http://dx.doi.org/10.2118/84288-pa>.

- Herrera, J. O., Jr., W. D. George, B. F. Birdwell et al. 1978. Wellbore Heat Losses In Deep Steam Injection Wells S1-B Zone, Cat Canyon Field. Proc., SPE California Regional Meeting, San Francisco, California. <http://dx.doi.org/10.2118/7117-MS>.
- Hoang, H. N., J. Mahadevan, H. Lopez. 2012. Injection Profiling During Limited-Entry Fracturing Using Distributed-Temperature-Sensor Data. *SPE Journal* **17** (3): 752-767. <http://dx.doi.org/10.2118/140442-pa>.
- Hong, K. C., S. Griston. 1986. New Methods for Controlled Injection of Steam Into Multiple Sands. Proc., SPE Annual Technical Conference and Exhibition, New Orleans, Louisiana. <http://dx.doi.org/10.2118/15472-MS>.
- Izgec, B., M. E. Cribbs, S. V. Pace et al. 2009. Placement of Permanent Downhole-Pressure Sensors in Reservoir Surveillance. *SPE Production & Operations* **24** (1): 87-95. <http://dx.doi.org/10.2118/107268-pa>.
- Izgec, B., A. R. Hasan, D. Lin et al. 2010. Flow-Rate Estimation From Wellhead-Pressure and -Temperature Data. *SPE Production & Operations* **25** (1): 31-39. <http://dx.doi.org/10.2118/115790-PA>.
- Izgec, B., C. S. Kabir, D. Zhu et al. 2007. Transient Fluid and Heat Flow Modeling in Coupled Wellbore/Reservoir Systems. *SPE Reservoir Evaluation & Engineering* **10** (3): 294-301. <http://dx.doi.org/10.2118/102070-pa>.
- Kabir, C. S., A. R. Hasan. 1998. Does Gauge Placement Matter in Downhole Transient-Data Acquisition?. *SPE Reservoir Evaluation & Engineering* **1** (1): 64-68. <http://dx.doi.org/10.2118/36527-pa>.

- Kabir, C. S., A. R. Hasan, D. L. Jordan et al. 1996. A Wellbore/Reservoir Simulator for Testing Gas Wells in High-Temperature Reservoirs. *SPE Formation Evaluation* **11** (2): 128-134. <http://dx.doi.org/10.2118/28402-pa>.
- Kabir, C. S., X. Yi, M. Jakymec et al. 2014. Interpreting Distributed-Temperature Measurements in Deepwater Gas-Well Testing: Estimation of Static and Dynamic Thermal Gradients, and Flow Rates. *SPE Production & Operations* **29** (2): 97-104. <http://dx.doi.org/10.2118/166333-pa>.
- Kabir, C. S., B. Izgec, A.R. Hasan et al. 2012. Computing Flow Profiles and Total Flow Rate with Temperature Surveys in Gas Wells. *Journal of Natural Gas Science and Engineering* **4**: 1-7. <http://dx.doi.org/10.1016/j.jngse.2011.10.004>.
- Larsen, L., K. Kviljo. 1990. Variable-Skin and Cleanup Effects in Well-Test Data. *SPE Formation Evaluation* **5** (3): 272-276. <http://dx.doi.org/10.2118/15581-pa>.
- Larsen, L., K. Kviljo, T. Litlehamar. 1990. Estimating Skin Decline and Relative Permeabilities From Cleanup Effects on Well-Test Data With Buckley-Leverett Methods. *SPE Formation Evaluation* **5** (4): 360-368. <http://dx.doi.org/10.2118/17566-pa>.
- Lesem, L. B., F. Greytok, F. Marotta et al. 1957. *A Method of Calculating the Distribution of Temperature in Flowing Gas Wells*, Society of Petroleum Engineers (Reprint).
- Moss, J. T., P.D. White. 1959. How To Calculate Temperature Profiles in a Water Injection Well. *Oil and Gas J* **57** (11): 174.

- Pacheco, E.F., S.M. Ali. 1972. Wellbore Heat Losses and Pressure Drop in Steam Injection. *Journal of Petroleum Technology* **24** (02): 139-144.
<http://dx.doi.org/10.2118/3428-PA>.
- Parta, P. E., A. P. Parapat, R. Burgos et al. 2010. A Successful Application of Fiber-Optic-Enabled Coiled Tubing With Distributed-Temperature Sensing Along With Pressures To Diagnose Production Decline in an Offshore Oil Well. *SPE Production & Operations* **25** (2): 204-210. <http://dx.doi.org/10.2118/121696-pa>.
- Ramaswami, S. R., H. Elshahawi, A. El-Battawy. 2012. Integration of Wireline Formation Testing and Well Testing Evaluation--An Example From the Caspian. *SPE Reservoir Evaluation & Engineering* **15** (3): 300-313.
<http://dx.doi.org/10.2118/139837-pa>.
- Ramey, H. J., Jr. 1962. Wellbore Heat Transmission. *Journal of Petroleum Technology* **14** (4). <http://dx.doi.org/10.2118/96-pa>.
- Sagar, R., D. R. Doty, Z. Schmidt. 1991. Predicting Temperature Profiles in a Flowing Well. *SPE Production Engineering* **6** (4): 441-448.
<http://dx.doi.org/10.2118/19702-PA>.
- Satter, A. 1965. Heat Losses During Flow of Steam Down a Wellbore. *Journal of Petroleum Technology* **17** (7): 845-851. <http://dx.doi.org/10.2118/1071-PA>.
- Schlumberger, M., H. G. Doll, A. A. Perebinosoff. 1937. Temperature Measurements in Oil Wells. *Journal of the Institution of Petroleum Technologists* **23** (159): 1-25.

- Shiu, K. C., H. D. Beggs. 1980. Predicting Temperatures in Flowing Oil Wells. *Journal of Energy Resources Technology* **102** (1): 2-11.
<http://dx.doi.org/10.1115/1.3227845>.
- Tabatabaei, M., D. Zhu. 2012. Fracture-Stimulation Diagnostics in Horizontal Wells Through Use of Distributed-Temperature-Sensing Technology. *SPE Production & Operations* **27** (4): 356-362. <http://dx.doi.org/10.2118/148835-pa>.
- Tan, X., M. Tabatabaei, D. Zhu et al. 2012. Diagnosis of Acid Placement From Temperature Profiles. *SPE Production & Operations* **27** (3): 284-293.
<http://dx.doi.org/10.2118/144194-pa>.
- Tardy, P. M. J., P. Ramondenc, X. Weng et al. 2012. Inversion of Distributed-Temperature-Sensing Logs To Measure Zonal Coverage During and After Wellbore Treatments With Coiled Tubing. *SPE Production & Operations* **27** (1): 78-86. <http://dx.doi.org/10.2118/143331-pa>.
- Theuveny, B. C., D. Mikhailov, P. Spesivtsev et al. 2013. Integrated Approach To Simulation Of Near-Wellbore and Wellbore Cleanup. Proc., SPE Annual Technical Conference and Exhibition, New Orleans, Louisiana.
<http://dx.doi.org/10.2118/166509-ms>.
- Wang, X., J. Lee, B. Thigpen et al. 2008. Modeling Flow Profile Using Distributed Temperature Sensor (DTS) System. *Amsterdam, The Netherlands: Society of Petroleum Engineers*. <http://dx.doi.org/10.2118/111790-MS>.
- WELLCAT Casing Design Software, Landmark, Halliburton. 2003.
<https://www.landmarksoftware.com/Pages/WELLCAT.aspx>.

Willhite, G. P. 1967. Over-all Heat Transfer Coefficients in Steam And Hot Water Injection Wells. *Journal of Petroleum Technology* **19** (5): 607-615.

<http://dx.doi.org/10.2118/1449-pa>.

Willhite, G. P., S. Griston. 1987. Wellbore Refluxing in Steam Injection Wells. *Journal of Petroleum Technology* **39** (3): 353-362. <http://dx.doi.org/10.2118/15056-PA>.

Witterholt, E.J., M.R. Tixier. 1972. Temperature Logging in Injection Wells. *San Antonio, Texas: Society of Petroleum Engineers*. <http://dx.doi.org/10.2118/4022-MS>.

APPENDIX A
PRESSURE DATA

Time, hr	Pressure, psig	Time, hr	Pressure, psig
0.95	4019.16	25.22	3971.07
1.45	4004.86	27.20	3999.16
1.97	3993.42	29.20	3958.17
2.45	3977.39	31.20	3952.16
2.95	3955.72	33.23	3948.99
3.45	3927.22	35.20	3946.95
3.95	3903.09	37.20	3906.81
4.73	3881.02	39.20	3899.01
7.22	3849.21	41.20	3894.55
8.70	3791.51	43.20	3891.37
9.72	3775.30	45.20	3849.36
11.12	3764.06	47.20	3841.68
11.72	3740.72	49.25	3836.85
14.22	3765.33	54.25	3832.54
16.72	3960.50	59.25	3777.66
19.22	3982.76	64.25	3767.32
21.72	3993.06	69.25	3760.65
23.72	3998.99	73.23	3755.52

Table A. 1 – Bottomhole pressure data, Well 2.

Time, hr	Pressure, psig	Time, hr	Pressure, psig
0.33	5530.65	33.71	5450.58
0.83	5521.14	35.71	5447.94
1.55	5515.04	37.71	5446.02
1.79	5494.01	39.71	5392.42
2.29	5489.82	41.86	5388.95
3.30	5469.19	53.86	5374.29
4.79	5428.48	65.86	5286.18
6.79	5372.36	77.86	5270.92
8.79	5322.12	90.45	5256.75
11.53	5322.48	90.64	5245.53
13.53	5315.69	90.66	5412.40
15.53	5501.27	90.68	5413.02
17.53	5506.85	90.69	5413.78
19.53	5509.92	90.73	5413.85
21.53	5511.88	90.80	5415.16
23.61	5513.31	93.80	5416.53
23.70	5514.43	96.80	5243.63
23.79	5514.46	99.80	5240.71
25.29	5492.10	102.80	5237.16
26.68	5501.86	105.80	5233.74
29.56	5490.51	108.80	5230.50
29.71	5488.43	113.49	5229.59
31.71	5488.47		

Table A. 2 – Bottomhole pressure data, Well 3.

Time, hr	Pressure, psig	Time, hr	Pressure, psig
0.93	6857.58	43.25	6719.27
1.76	6735.19	43.75	6746.32
2.38	6934.04	45.75	6686.23
4.38	6816.50	47.75	6635.77
6.96	6714.94	49.75	6642.97
8.96	6615.14	51.75	6682.03
10.96	6903.56	52.75	6749.91
12.96	6919.98	53.25	6751.86
14.96	6927.28	54.00	6740.80
16.77	6931.52	56.00	6645.28
17.75	6933.58	58.00	6620.58
18.00	6895.88	60.00	6600.35
18.25	6881.37	62.00	6593.92
21.50	6901.64	64.00	6589.04
23.50	6889.26	67.50	6584.84
25.50	6863.32	67.75	6574.91
27.25	6833.14	73.75	6574.26
29.25	6827.52	79.75	6569.40
31.25	6743.17	85.75	6583.66
33.25	6732.68	91.75	6575.28
35.25	6727.23	97.75	6570.60
37.50	6722.74	103.75	6564.89
39.50	6713.54	109.81	6551.61
41.75	6654.25		

Table A. 3 - Bottomhole pressure data, Well 4.

APPENDIX B

SAMPLE CALCULATION

New methodology proposed in this work is calculation intensive; here we present some details of computations so that others can replicate our results or implement the model. The calculations are shown for Well 4. Input parameters for Well 4 are presented in Table 5. The depth of 3,777 ft is selected for the sample calculations. At this depth, the measured and estimated quantities are given below. Some parameters like the velocity gradient and dZ/dT are required for the calculation of ϕ . The velocity gradient is calculated numerically. The Z-factor and its temperature derivative are calculated using the Dranchuk and Abou-Kassem correlation (1975). The calculation uses the Newton-Raphson approach for iterative calculations. The parameters obtained at 5.5 hours are shown in Table B.1 and B.2.

Bottomhole pressure, psig	6,669
Fluid temperature, °F	173.9
Flow rate, MMscf/D	47.36

Table B. 1 – Measured quantities at 5.5 hours in Well 4.

U, Btu/(hr-ft ² -°F)	3.12
v _f , ft/sec	22.84
dv/dz, 1/sec	0.000181
Z	1.002
dZ/dT, 1/°F	0.00054
C _J C _p , ft ³ /lb _m	0.0232
ϕ	-0.00064
Ψ, °F/ft	0.0126
ξ, °F/ft	0.00033

Table B. 2 - Calculated quantities at 5.5 hours in Well 4.

By using these values, the fluid temperature is calculated to be 172.6 °F, which compares well to the measured temperature. Rate is estimated using an optimization technique whereby the difference between the calculated and measured temperatures is minimized. The optimization yields a rate of 46 MMscf/D. Note that this calculation is performed for a time during the cleanup phase. During this time, the fluid properties are not only changing with pressure and temperature but are also expected to change as a result of early production of mud filtrate and/or completion fluid, which could vary with time in certain instances. Therefore, a greater tolerance of temperature match might be required in those rare instances.

The temperature calculated without accounting for superposition was 172 °F. The superposition calculation, although more accurate, does not bring about a large difference in the calculation without superposition. This point is also alluded to in the

text. The crux of the difference lies in how significant the value of ζ is. In this case, it is not significant. Hence, the two temperatures are about the same.